Nanocellulose-based systems for the removal of perfluoroalkyl compounds from water

by

Iflah Shahid

A thesis

presented to the University of Waterloo

in fulfillment of the

thesis requirement for the degree of

Master of Applied Science

in

Chemical Engineering

Waterloo, Ontario, Canada, 2021

AUTHOR'S DECLARATION

I hereby declare that I am the sole author of this thesis. This is a true copy of the thesis,

including any required final revisions, as accepted by my examiners.

I understand that my thesis may be made electronically available to the public.

Abstract

The contamination of drinking water sources with poly- and perfluoroalkyl substances (PFAS) is a cause for concern. These compounds have been linked to several health problems in humans, and thus there is an urgent need to develop sustainable removal technologies for PFAS remediation. Cellulose nanocrystals (CNCs) are derived from plants and offer a sustainable, green approach for the development of adsorbents due to their ease of modification. The modification of CNCs with glycidyltrimethylammonium chloride (GTMAC) and the lignin-based flocculant, Tanfloc, was used to prepare positively charged CNCs, while beta cyclodextrin (β-CD) was grafted onto CNCs to promote hydrophobic interactions between PFAS and β-CD. TF-CNC was incorporated into sodium alginate hydrogel beads for ease of adsorption and removal.

Treatment of an anionic dye, methyl orange (MO), with the adsorbents resulted in a maximum adsorption capacity of 125.7 mg/g for β-CD-CNC, and up to 80% removal of 1000 ppm MO by GTMAC-CNC. TFSH-CNC and TFSG-CNC resulted in q_{max} values of 917.8 mg/g and 247.5 mg/g, respectively, while the q_{max} values of ALG beads impregnated with TF-CNC increased from 2.2 mg/g to 4.9 mg/g. Treatment of KPFBS with the adsorbents resulted in removal percentages ranging from 26.1 to 56.5%, indicating that chemical and physical modifications improve the adsorption capacity of CNCs for PFAS. Together, these results indicate that modified CNCs offer a promising template for the development of adsorbents for PFAS remediation from water sources.

Acknowledgements

Table of Contents

List of Figures

x

List of Tables

Chapter 1: Introduction

1.1 Project Motivation

Per- and polyfluoroalkyl substances (PFASs) are a group of highly persistent contaminants that have garnered growing interest and concern over the past few decades [1]. Due to their chemical stability and surfactant-like characteristics, these compounds are extremely difficult to break down [2], and have thus become ubiquitous in the environment [3]. The persistent nature of PFASs is of major concern due to the possible links of various PFASs with several forms of cancer [4], diabetes [5], and immune-suppression [6]. Thus, there exists an urgent need to develop efficient PFAS removal techniques from the environment.

Current methods for the removal of PFASs from water include the use of granular activated carbon (GAC), ion exchange resins, and membrane separation processes such as reverse osmosis (RO) and nanofiltration (NF) [7]. Several issues such as high installation and maintenance costs [8], large environmental impact due to high temperatures for activation [9], as well as fouling and scaling of membranes [10], require that focus shift toward sustainable and efficient PFAS removal methods.

Natural materials, such as cellulose, alginate, lignin, and cyclodextrins provide a sustainable and 'green' approach for the development of new PFAS removal systems. Since these materials are derived from plant material, they are environmentally friendly and can be used to formulate processes that rely less heavily on synthetic chemicals which may raise additional toxicity concerns.

1.2 Project Outcomes

The overall aim of this project is to develop sustainable adsorbents for the removal of PFASs from water. Two approaches were adopted to achieve this goal: chemical modification of cellulose nanocrystals (CNCs) and the coating of CNCs.

The chemical modification of CNCs was further divided into two directions. The first involved the introduction of cationic groups on the CNC surface to allow electrostatic attraction between the negatively charged PFASs and positively charged CNCs. The second method involved the grafting of β-cyclodextrin (β-CD) onto the CNC surface to allow for the formation of inclusion complexes with PFASs [11].

Coated CNCs were prepared using the lignin-based, cationic flocculant Tanfloc. The coating was produced to take advantage of electrostatic attraction between the coated CNCs and PFASs. Both the chemically modified and coated CNCs were tested for the removal of the anionic model compound, methyl orange, and potassium perfluorobutanesulfoanate (KPFBS) from water to determine the adsorption efficiency of the generated materials and their potential application for PFAS removal.

1.3 Thesis Outline

This thesis consists of five chapters. Chapter 1 contains an introduction to the project and provides the motivation for the study. Chapter 2 provides a brief literature review on PFASs, PFAS removal techniques, and the reasoning behind the material selection for this study. Chapters 3 and 4 contain experimental data and results, with Chapter 3 focusing on chemically modified CNCs and Chapter 4 focusing on coated CNCs. Finally, Chapter 5

provides overarching conclusions that can be drawn from this study and provides recommendations for future work on PFAS removal from water.

Chapter 2: Literature Review

2.1 Poly- and Perfluoroalkyl Substances

Poly- and perfluoroalkyl substances (PFAS) are defined as aliphatic compounds containing one or more carbon atoms, with all the hydrogen atoms substituted with fluorine [3]. All PFAS contain the perfluoroalkyl moiety, defined by the formula C_nF_{2n+1-}. Perfluoroalkyl substances differ from polyfluoroalkyl substances in that they have all their non-functional group hydrogen atoms replaced with fluorine, whereas polyfluoroalkyl substances only have some carbon atoms with all their hydrogen atoms replaced with fluorine. Several classes of PFAS exist, and almost 8000 distinct compounds belonging to this family of chemicals are included in the United States Environmental Protection Agency PFAS master list [12]. Figure 1 shows the difference between PFAS and non-PFAS compounds.
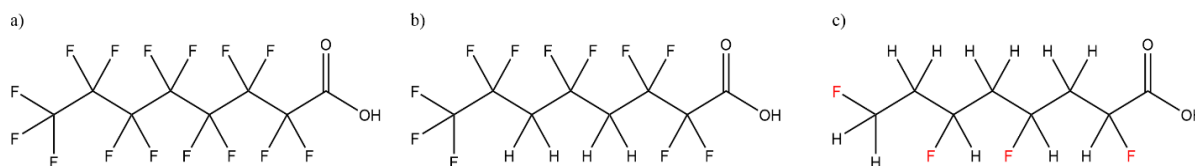
Figure 1: Examples of a) a perfluoroalkyl substance, with all hydrogen atoms replaced with fluorine atoms, b) a polyfluoroalkyl substance, with some carbon atoms fully saturated with fluorine atoms, and c) a compound with scattered hydrogen atoms replaced with fluorine atoms. Both a) and b) are PFASs, but c) is not.

2.2 General Properties of PFAS

Due to their chemical structure, PFAS tend to be more surface active than ordinary surfactants, and the strength of the carbon-fluorine bond makes them highly resistant to acidic, alkaline, oxidative, and reductive reagents, as well as to high temperatures [2]. PFAS can also withstand photolytic, microbial, and metabolic degradation processes, leading to their highly persistent nature in the environment [13]. PFAS exhibit both hydrophobic and hydrophilic

behaviour due to the low polarizability of the fluorine atoms, and become increasingly inert with increasing carbon chain length [14].

In general, PFAS solubility decreases with increasing carbon chain length due to the increase in hydrophobicity of long chain compounds [14]. The solubility is also dependent on the counterion present, with most anions being more soluble than the free acid at a given temperature [2]. Predicted and experimental pKa values for the perfluoroalkyl carboxylic acids (PFCAs) and the perfluoroalkyl sulfonic acids (PFSAs) indicate that these groups are strong acids, and will tend to dissociate at environmentally relevant pH conditions [13]. However, other classes of PFAS, such as fluorotelomer alcohols (FTOHs), tend to remain in their undissociated form at environmentally relevant pH conditions, indicating that different methods may be required to remove different PFAS from environmental matrices.

2.3 Occurrence and Hazardous Potential of PFAS

PFAS have become ubiquitous in the environment due to their widespread use in consumer and industrial products. Because of the historical and current use of PFAS, the compounds have been found in sediment cores in Arctic Lakes in Canada [15], surface water and sediment in the North and Baltic Seas in Europe [16], household and childcare center dust [17], [18], seafood [19], agricultural plants [20], bird eggs [21], and drinking water [22]. Exposure of humans to PFAS through water, food, consumer products, and dust has led to the prevalence of PFAS in human blood serum [23], tissues [24], breast milk, and urine [25].

Although some manufacturers have phased out the production of C-8 PFAS such as perfluorooctanoic acid (PFOA) and perfluorooctanesulfonic acid (PFOS), production continues in several countries including China, India, Poland, and Russia [15]. After the ban

on long chain PFASs, the focus shifted to the manufacture of alternatives such as short chain PFAS, which may be just as harmful than their phased-out precursors. These short chain PFASs are already being detected in increasing quantities in breast milk, suggesting that human exposure to these PFAS is increasing [26]. The cumulative exposure to PFASs, combined with emerging evidence that short chain PFASs are linked to thyroid dysregulation in newborn girls [27] and disturbances in fetal gonadotrophins [28] is a cause for concern. Furthermore, long chain PFAS still exist in the environment and are linked to health risks including depressed immune function and reduced effectiveness of vaccines [6], [29], [30], increased risk for diabetes [5], increased oxidative stress [31], liver and kidney diseases [29], and cancer [32].

A study on the accumulation of PFASs in human tissues showed that various PFASs accumulate differentially in different tissues (Figure 2) [24]. Acidic PFASs with odd number carbon-chains accumulate in the kidneys, while even number carbon-chain compounds and sulphonates accumulate in the brain. Sulphonates can also accumulate in bone. People in older age groups tend to have higher PFAS accumulation in their tissues, suggesting that PFASs accumulate in tissues over time and can lead to adverse health effects with increasing age.

With exposure to PFAS beginning prenatally and continuing over a lifetime, it is essential to develop efficient PFAS remediation methods to reduce human exposure to PFAS and the health effects that come with it.
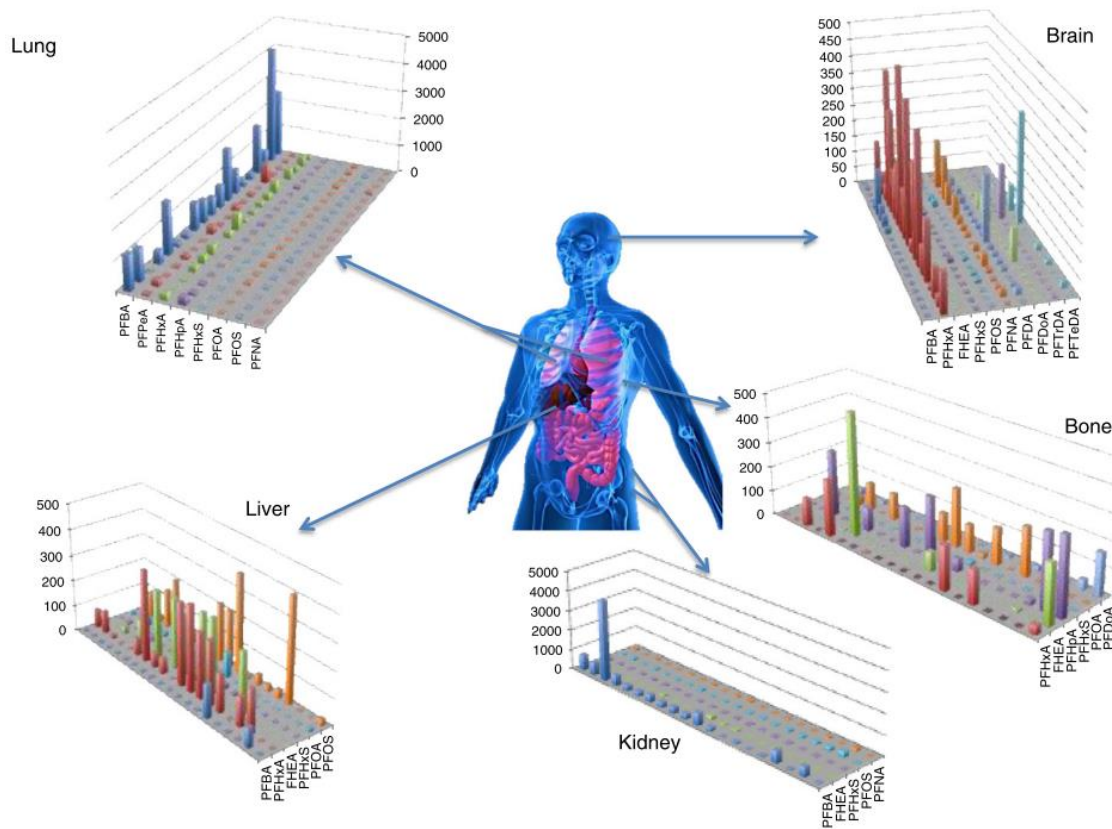
Figure 2: Concentrations of various PFASs (ng/g) in 5 human tissues. Figure from reference [24].

2.4 PFAS Adsorption

2.4.1 Mechanism

The predominant mechanisms for PFAS removal through adsorption are hydrophobic and electrostatic interactions [33]. The anionic head of PFASs can be adsorbed onto positively charged adsorbents through electrostatic interactions (Figure 3). However, if negatively charged natural organic matter (NOM) is present in the water to be treated, the organic matter may compete with the PFASs and reduce the adsorption efficiency of the adsorbent. The repulsion between NOM and PFASs can also reduce the electrostatic interaction between

9

PFASs and positively charged adsorbents. Conversely, the presence of multivalent cations in water samples can increase the adsorption efficiency of adsorbents by acting as a bridge between the adsorbent and the PFASs.

Hydrophobic interactions are also significant for the adsorption of PFASs on various adsorbents [33]. The hydrophobic tails of PFASs self-organize to form micelles in bulk water to reduce the entropy of the system. This interaction is important at high pH values near and above the point of zero charge of positively charged adsorbents. Many carbonaceous and resin adsorbents rely on hydrophobic interactions as the main method of PFAS removal from water.

The formation of micelles and hemi-micelles on surfaces has also been reported on PFAS adsorption [33]. Micelles and hemi-micelles can both enhance and inhibit the adsorption of PFAS on an adsorbent. On one hand, the formation of these structures can attract more PFAS molecules to the surface of the adsorbent, thus enhancing the removal, while on the other hand, the micelles and hemi-micelles can block the pathway to the surface for other molecules in solution, which can reduce the adsorption capacity. This is particularly important in microporous adsorbents, where pores might become blocked by micelles and hemi-micelles.

Besides electrostatic and hydrophobic interactions, ligand and ion exchange are also pathways for PFAS adsorption, particularly when metal hydroxides and oxides are present [33]. Anions and functional groups such as hydroxyl groups can form inner-sphere complexes or act as exchange ions with the head groups of PFASs. Despite the hydrophobicity of PFASs,
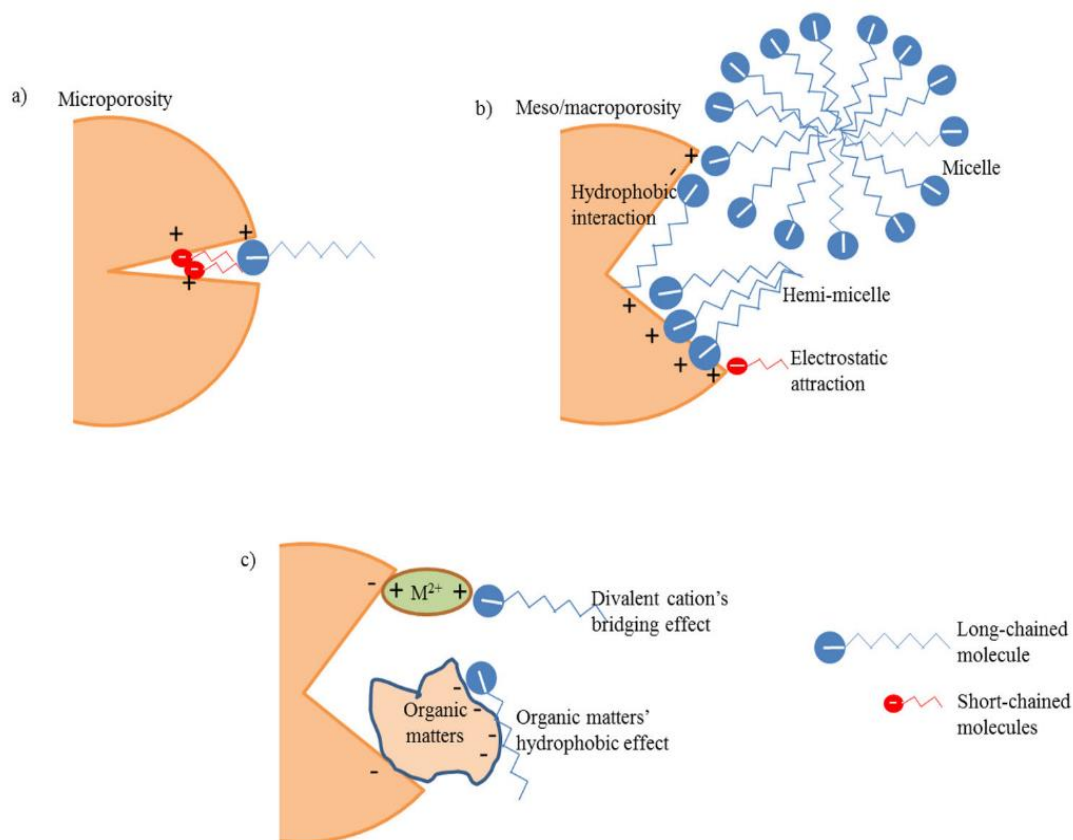
Figure 3: Adsorption mechanisms for PFAS. In a) microporous materials, short-chain PFASs can diffuse into the pores, while long-chain PFASs may block the pores; b) meso/macroporous materials can allow diffusion of both long and short-chain PFASs into the pores and can also result in the formation of micelles and hemi-micelles; c) the presence of natural organic matter and multivalent cations can result in the reduction or enhancement of the interactions between PFASs and the adsorbent. Figure adapted from reference [33].

hydrogen bonding between hydroxyl groups and the fluorine atoms of PFASs has been reported. However, this hydrogen bonding can easily be displaced by water molecules if the adsorbent contains many protonated groups and is thus usually insignificant in PFAS adsorption.

2.4.2 Adsorption Isotherms

Adsorption isotherms are plots of the equilibrium relationship between the amount of compound left in solution and the amount of compound on the surface of an adsorbent [34]. The two commonly used models applied to adsorbents in water treatment are the Langmuir and Freundlich adsorption isotherms.

The Langmuir isotherm (Figure 4a) assumes monolayer adsorption, with no or only ideal interactions between the adsorbate particles [35]. The adsorbent surface is assumed to be homogeneous, and all the adsorbing sites are considered chemically equivalent, with only one particle able to adsorb to each site. Additionally, the adsorbate is assumed to occupy an immobile state so it will be bound to one site and remain adsorbed until it desorbs. The relative coverage of the adsorbent surface and the adsorption density, Γ (units of mol/g-adsorbent), are described by the following equations:

$$\theta = \frac{K_L P}{1+K_L P} \tag{Eq. 1}$$

$$\theta = \frac{\Gamma}{\Gamma_{mono}} \tag{Eq. 2}$$

$$\Gamma = f(P/c, T) \tag{Eq. 3}$$

Here, θ represents relative coverage, K_L is the Langmuir constant, Γ_{mono} is the maximum amount adsorbed, and P/c are the pressure or concentration of the sample. The Langmuir adsorption isotherm describes saturation at high concentrations when the full monolayer is achieved, and this behaviour is often observed in solutions and when porous materials are used [35].

The Freundlich adsorption isotherm (Figure 4b) applies when the adsorbent surface is heterogeneous and contains sites that are occupied at different rates. Repulsion between

adsorbate molecules can also occur in this case. The adsorption function is described by the following equation, where K_F and q are constants for a given adsorbate and adsorbent:

$$\Gamma = K_F . P^q \hspace{6cm} \text{(Eq. 4)}$$

a
b
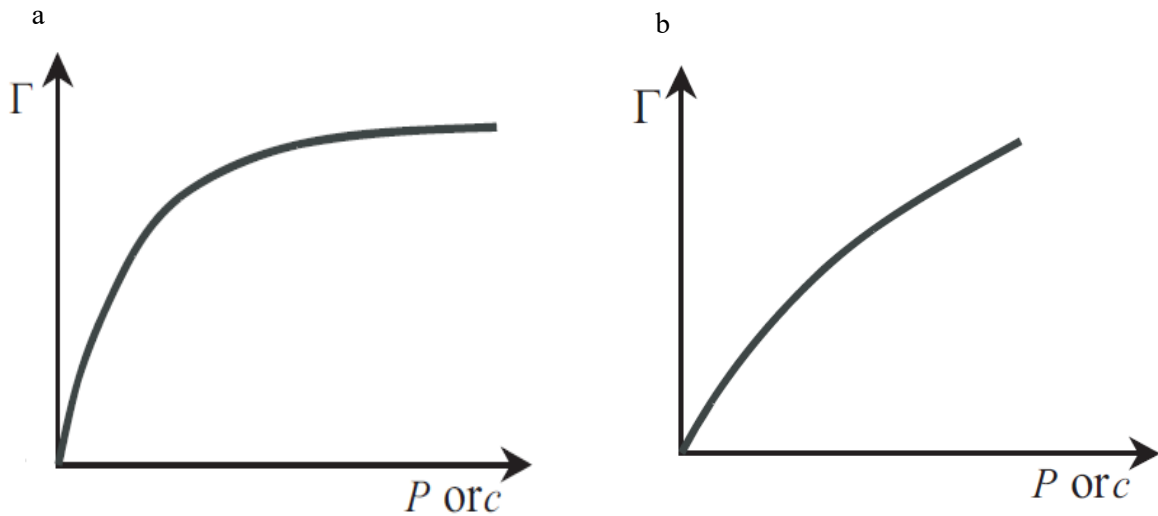
Figure 4: The a) Langmuir and b) Freundlich adsorption isotherms. Figure adapted from reference [35].

2.5 Current PFAS Removal Methods

Due to the inertness and resistance of PFAS to physical, chemical, and biological degradation, current water treatment methods that are effective for PFAS removal are based on adsorption and filtration. It must be noted that several of these treatment methods are not specifically designed for PFAS removal in full scale water treatment plants but have been found to be effective at removing them.

2.5.1 Activated Carbons

Activated carbons are carbonaceous adsorbents that include both granular activated carbon (GAC) and powdered activated carbon (PAC). While both these adsorbents are used in

water treatment plants for the purpose of removing taste and odour in drinking water, they are also known to be effective against synthetic organic chemicals, including PFASs [34].

Activated carbon can be prepared from various materials including bituminous coal, bones, coconut shells, lignite, peat, pecan shells, petroleum-based residues, pulp mill black ash, sugar, wastewater treatment sludge, and wood [34]. Today, lignite, coal, and coke are commonly used to produce activated carbon. The structure of activated carbon is more disorganized but similar to pure graphite. Typical activated carbons have micropores, transitional pores, and macropores, with some macropores leading to the particle surface.

Activated carbon is produced through physical or chemical activation. In physical activation, the material undergoes carbonization upon being pyrolyzed at very high temperatures (600-900 °C) [9]. Following pyrolysis, the char is gasified or activated with steam, carbon dioxide, air, or a combination of all of these at temperatures around 600-1200 °C. In chemical activation, the precursor material is impregnated with concentrated salts, acids, or bases, and is then heated. Chemical activation is known to impart better micro and mesopore volumes and tends to be more consistent than physical activation.

Despite their use in water treatment plants, the efficiency of PFAS removal by activated carbon is dependent on several factors. Studies have shown that the renewal efficiency of GAC filters decreases steadily over time [36], [37], with PFAS breakthrough occurring as early as 42 days after the introduction of a new filter [38]. Factors such as the weather also have an effect on PFAS removal efficiency, with much greater desorption occurring during summer as compared to winter [37]. This effect can be significant enough to cause negative removal ratios during summer. Finally, activated carbons are much more efficient at removing long chain

14

PFAS than short chain PFAS, due to the significance of the hydrophobic mechanism of adsorption [39].

2.5.2 Ion-Exchange Resins (IEX)

Besides activated carbon, a commonly used PFAS removal method in current use is anion exchange resins. These resins have shown good removal efficiencies for PFAS, but the removal efficiency is highly dependent on the type of resin and its properties.

Polyacrylic resins perform better than resins with polystyrene matrices due to the higher hydrophilicity of the matrix, which allows easier transport of PFAS into the resin pores [40]. Additionally, polyamine resins tend to be effective over a narrower pH range (3 to 9), whereas quaternary ammonium resins are effective over a broader pH range due to a permanent positive charge on the quaternary ammonium group. Similar to activated carbons, IEX are more effective at removing long chain PFAS compared to short chain PFAS due to increasing hydrophobic interactions between the resin and the carbon chain [41]. Furthermore, long chain compounds are less soluble in water and have a greater tendency to adsorb. The chain length of the resin functional group also affects the removal efficiency, with longer chain lengths increasing the selectivity for larger and more hydrophobic anions such as long chain PFAS.

2.5.3 Nanofiltration and Reverse Osmosis Membranes for PFAS Removal

Nanofiltration (NF) and reverse osmosis (RO) are techniques that have been shown to be effective for PFAS removal and are in use in current water treatment technology. Nanofiltration is a filtration technique that requires the use of pressure to remove unwanted substances from water using a membrane with very small pore sizes (1 to 10 nm) [42]. The removal mechanisms usually include size exclusion as well as electrostatic interactions.

Reverse osmosis is a filtration process that is essentially the opposite of osmosis [42]. In osmosis, the solvent naturally moves from an area with low solute concentration to an area with high solute concentration to reduce the Gibbs free energy of the system. In reverse osmosis, an external pressure is applied to force the solvent to travel in an opposite direction than it would during osmosis. Reverse osmosis membranes typically have very small pore sizes, from 0.1 to 1 nm, and are thus capable of separating very small particles from water.

Studies on the effectiveness of RO treatment on PFAS-contaminated water in full scale water treatment plants have shown rejection of greater than 99% of PFAS in water [43], [44]. Bench scale studies have also shown greater than 99% rejection of PFOS from semiconductor wastewater [45]. Furthermore, RO membranes at the full scale have shown greater than 90% rejection of short chain PFAS such as perfluorobutanesulfonic acid (PFBS), which are typically difficult to remove using other techniques [43].

Bench scale studies on commercial NF membranes have shown that these membranes can achieve greater than 93% removal for both long chain and short chain PFAS [46]. A pilot plant study on PFAS removal reported that NF membranes achieved greater than 99% removal of PFAS from raw water, including short chain PFAS such as perfluorobutanoic acid (PFBA) [47]. A study on NF membranes with bipiperidine as one monomer and trimesoyl chloride as the other reported rejection of sulfate anions and permeation of cations to reduce scaling, showing that these membranes may be effective against anionic PFAS [48]. Another study on multilayer NF membranes reported PFOA and PFOS retention rates similar to commercial membranes, while also showing a reduction in scaling [49]. These multilayer membranes also had a much lower flux reduction compared to the commercial membrane (13% vs 37%),

16

indicating that these NF membranes may have longer filtration lifetimes than commercial membranes.

2.5.4 Disadvantages of Current Removal Methods

Activated carbon adsorbents such as GAC have high installation and maintenance costs, and negative environmental impact associated with them. For example, the installation of five new GAC filters in Plainfield Township, Michigan, cost $750,000 [8] and the annual GAC operation cost at a drinking water treatment plant in Uppsala, Sweden is 712 million Euros, with the majority of the cost attributed to GAC regeneration [50]. Apart from the high costs associated with GAC filters, regeneration requires very high temperatures that causes loss of material and have a negative environmental impact due to the energy cost and generated heat. Finally, the efficiency of GAC filters is dependent on dissolved organic matter, competing ions, weather conditions, and decreases as they age.

NF and RO processes also have high costs associated with them [43], such as the $137 million reverse osmosis upgrade and $2.9 million annual operating costs at a water treatment plant in Brunswick Country, North Carolina [8]. Other issues typically associated with filtration membranes include scaling, which reduces flux and leads to higher operational costs. The membranes are also subject to fouling, which can result in biofilm formation and release unwanted microbes into the water supply [10]. Finally, these membranes are also affected by several parameters such as pH, pressure, and membrane properties, which can affect PFAS rejection.

Due to the costs and problems associated with current treatment technologies, new PFAS removal methods are being developed and studied, with a focus toward the use of biomaterials, a few of which are discussed in the following section.

2.6 Biomaterial Adsorbents for PFAS Removal

With increasing concern over the negative impact of industrial processes on the environmental and the push toward more sustainable processes, several biomaterial-based adsorbents are being investigated for water treatment applications. These include both biomaterial-based activated carbons and biochar, as well as novel adsorbents based on functionalized biomaterials.

2.6.1 Biomaterial-Based Activated Carbon and Biochar

Activated carbons derived from bamboo, coconut-shell, and rice husk have gained attention since they are derived from agricultural products rather than fossil fuels. A comparison of bamboo-derived GAC (BAC) to coal-derived GAC (CAC) reported 70% PFOA removal by BAC and 30% removal by CAC [51] (Figure 5a). The PFOA removal efficiencies remained consistent over pH values from 2 to 9, and the BAC could be regenerated and used over 5 cycles with an overall reduction of PFOA removal by about 15% (Figure 5b), suggesting that agriculturally derived GAC may be a good alternative to coal- and petroleum-based GAC.

An alternative to GAC that has been generating interest is biochar, a low-cost carbon residue derived from the pyrolysis of wet biomass in an oxygen-limited environment [52]. Unlike activated carbon, biochar does not require harsh chemicals for treatment, and is much more environmentally friendly, requiring 6.1 MJ/kg for production and releasing 0.9 kg CO_2/kg, as compared to an energy demand of 97 MJ/kg and greenhouse gas emissions of 6.6
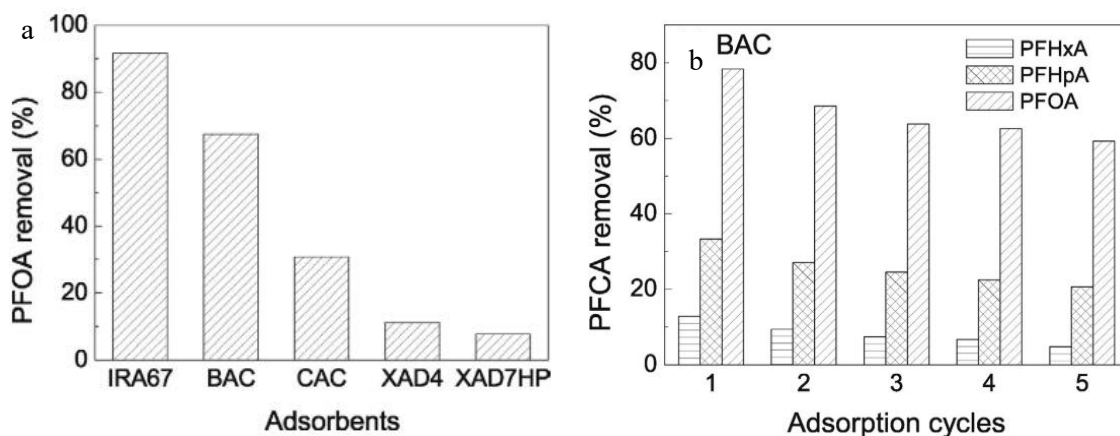
Figure 5: a) PFOA removal efficiencies of BAC, CAC, commercial IEX resin IRA67, macroporous styrene XAD4, and macroporous aliphatic acrylic polymer XAD7HP, and b) PFAS removal efficiency of BAC over 5 adsorption cycles. Figure from reference [51].

kg CO_2/kg by activated carbon. Further, biochar is much cheaper than activated carbon, with a cost of $256/ton compared to a production cost of $1500/ton for activated carbon [53]. Biochar has been reported to have maximum adsorption capacities of 21.6 mg/g, 35.2 mg/g, 10.3 mg/g, and 7.0 mg/g for PFOA, PFOS, PFBA, and PFBS, respectively. The magnetic modification of biochar has shown to produce a regenerable adsorbent material with maximum adsorption capacities of 204.7 mg/g for PFOA and 195.5 mg/g for PFOS [54]. These adsorption capacities are comparable to GAC, suggesting that biochar may be a viable option for PFAS removal in water treatment systems.

2.6.2 Natural Polymer-Based Adsorbents

With the shift toward deriving carbonaceous adsorbents from plantsinterest has also been shown in the use of using bio-based polymers as adsorbents for PFAS. These natural polymers include chitosan, starch, cyclodextrin, and cellulose.
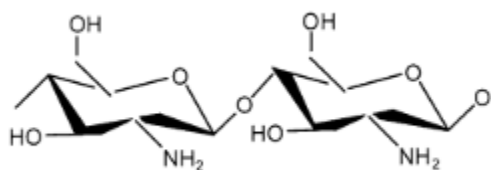
Figure 6: Structure of chitosan. Adapted from reference [55].

Chitosan (Figure 6) is a biopolymer derived from the deacetylation of chitin, which is extracted from shrimp and other crustaceans [55]. Free amino groups are present in chitosan, which becomes positively charged at low pH values, allowing for electrostatic interactions with anionic species such as acidic PFAS [56]. Studies on chitosan-based molecularly imprinted polymers (MIPs) have indicated the selective removal of up to 60% of the target PFAS, with recyclability over five cycles with no loss in the adsorption efficiency (Figure 7a-b) [57]. Epichlorohydrin-crosslinked chitosan beads have been reported to have maximum adsorption capacities of up to 2500 mg/g for PFOA [58], while chitosan-ethylene glycol hydrogels have shown a maximum adsorption capacity of 1200 mg/g for PFOA [59]. While these studies show favourable adsorption capacities, chitosan-based adsorbents are limited by pH, and become less effective as pH increases.
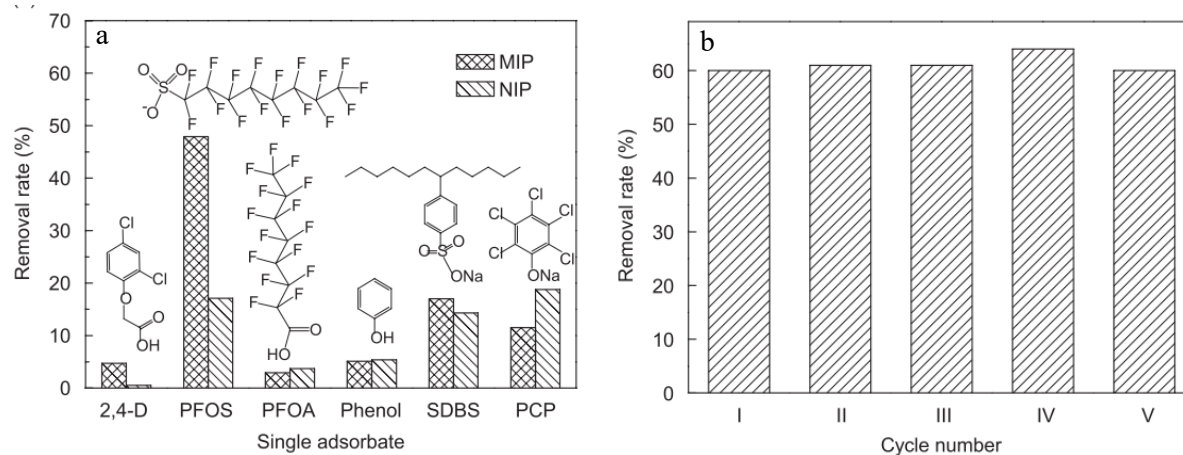
Figure 7: a) selective removal of PFOS by PFOS-templated chitosan MIPs and b) the PFOS removal efficiency of the MIPs over 5 regeneration cycles. Figure from reference [57].

Starch, an important energy storage polymer found in plants, is a homopolymer of α-glucopyranose units [60]. Starch has been shown to stabilize magnetite nanoparticles, which tend to agglomerate in solution [61]. The addition of 1% starch by weight to a ferrous-ferric solution was used to produce highly stabilized magnetite nanoparticles that achieved up to 62% PFOA from a sample solution, with a maximum adsorption capacity of 62.5 mg/g.

Another natural polymer of interest is cellulose, the most abundant polymer in the biosphere [62]. It is found in plants, animals, algae, fungi, and bacteria. Cellulose consists of glucose molecules connected by β-1,4-glycosidic linkages (Figure 8). In native cellulose, each glucose unit has three free hydroxyl groups on carbons 2, 3, and 6, which can be functionalized through various chemical reactions. Native cellulose can be converted to micro- and nano-forms using various top-down and bottom-up techniques. Cellulose has been studied for the removal of dyes, heavy metal ions, and other organic contaminants such as drugs from water, but few studies on the removal of PFAS using cellulose-based systems have been reported.

Different plant sources contain different amounts of cellulose by weight, with wood typically containing 40-50% cellulose, while cotton contains up to 90% cellulose by weight
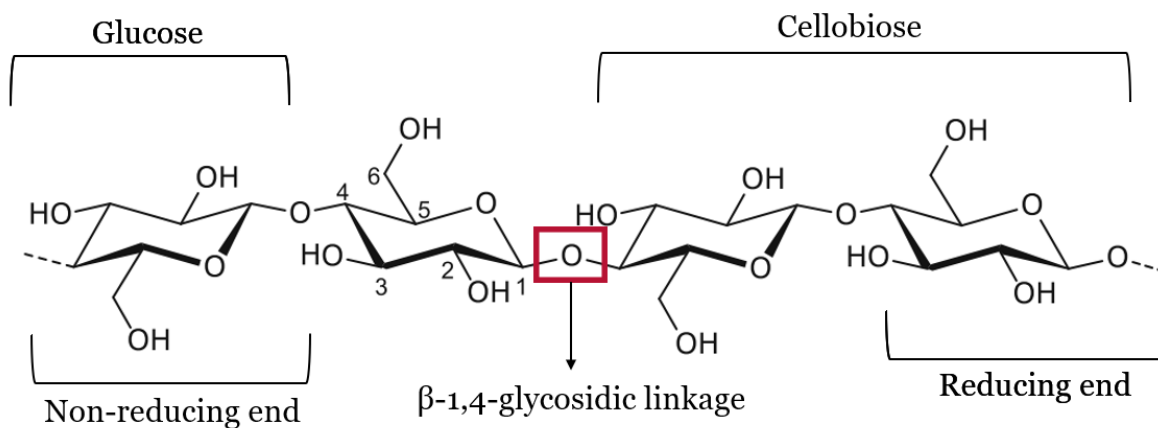
Figure 8: Structure of cellulose. Adapted from reference [62].

[62]. The introduction of quaternary ammonium groups into cotton can impart a permanent positive charge to the cotton, making it favourable for electrostatic interactions with anionic PFAS. Cotton quaternized with poly(2-(dimethylamino)ethyl methacrylate) has been reported to have maximum adsorption capacities of 1283 mg/g and 1650 mg/g for PFOA and PFOS, respectively [63]. Further, due to the permanent positive charge, the material is effective over a wide pH range. Despite the promise of quaternized cotton as an adsorbent for PFAS, it must be noted that cotton is an extremely energy- and labour-intensive crop with a significant environmental impact. Approximately 25% of the world's insecticides and 11% of the world's pesticides are used for cotton production [64], making cotton-based PFAS removal best suited when using recycled cotton or used textiles to reduce the environmental impact.

The use of cellulose from plants native to a geographic region provides a good alternative to using cotton-based adsorbent materials. Fiber obtained from the *Calotropis gigantea* plant, a plant native to South Asia, Southeast Asia, and North Africa, can be functionalized with polyaniline for the removal of PFOA from water [65]. This material has been reported to have a maximum adsorption capacity of 232.8 mg/g for PFOA, maintaining over 80% removal over 5 regeneration cycles.

Besides native cellulose, micro- and nanocellulose can also be functionalized for the development of adsorbents for PFAS removal. Cellulose microcrystals functionalized with polyethyleneimine (PEI) have been shown to achieve 90% PFOA removal, with a maximum adsorption capacity of 2.32 mg/g [66]. The adsorbent achieved up to 99% removal of 22 different PFAS from environmental lake water samples, and maintained its removal efficiency over 8 regeneration cycles, making it highly reusable (Figure 9a-b).

22
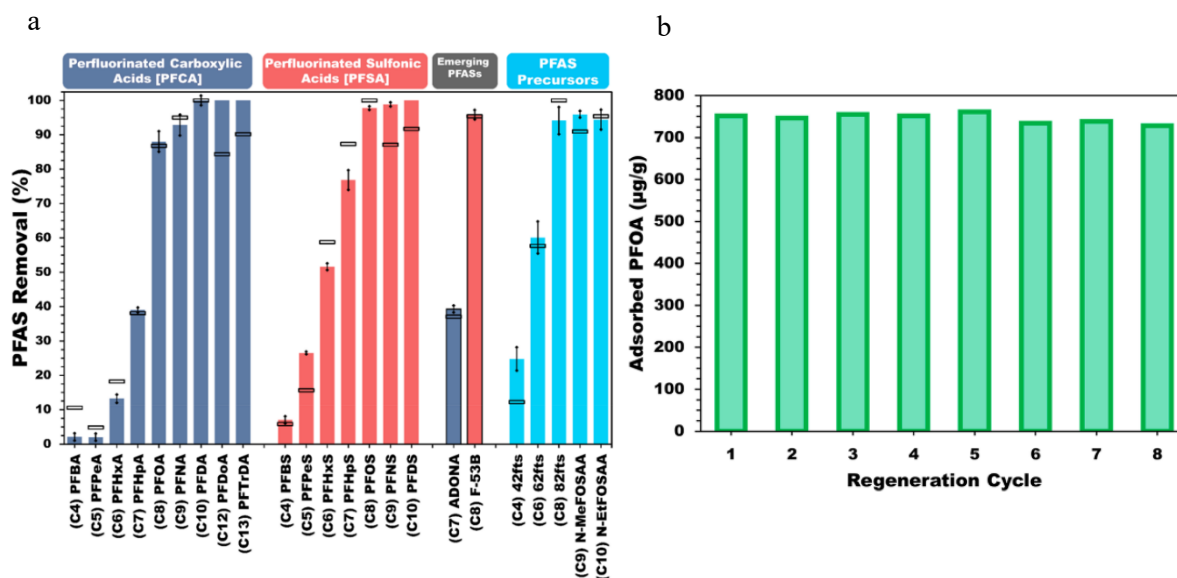
Figure 9: The a) removal of 22 different PFAS from lake water samples (coloured bars) and distilled water (open rectangles) using 25 mg/L functionalized cellulose microcrystals and b) the adsorption of PFOA over 8 adsorption cycles. Figure from reference [66].

Finally, cyclodextrins (Figure 10), cyclic oligosaccharides formed through the bacterial digestion of cellulose [67], have also garnered attention for PFAS removal from water. Magnetic nanoparticles functionalized with β-cyclodextrin (β-CD) and ionic liquid have been reported to remove both PFAS and Cr(VI) ions from sample solutions [68]. The functionalized
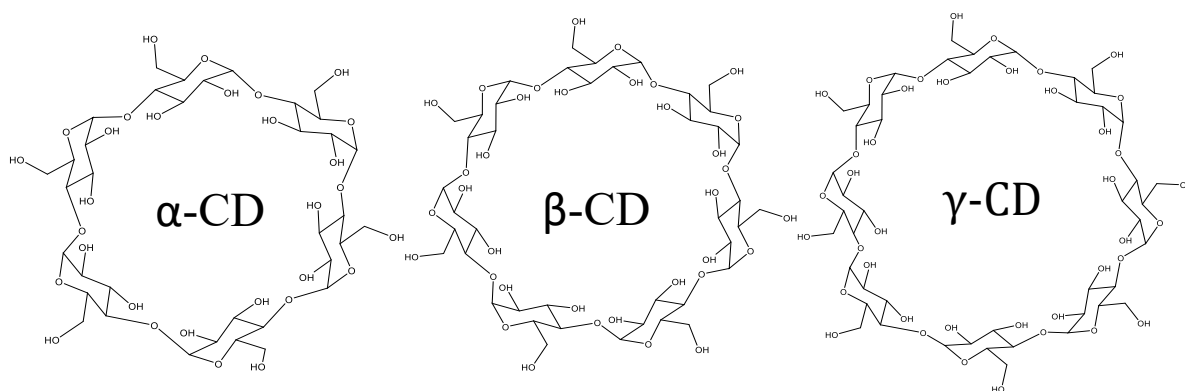
Figure 10: Structure of alpha, beta, and gamma cyclodextrin. Figure generated by author.

nanoparticles were able to achieve level of removal of PFOS and PFOA comparable to commercial activated carbon and maintained their removal efficiency over 10 regeneration cycles. β-CD polymers crosslinked with decafluorobiphenyl (DFB) have been shown to outperform commercial coconut-shell activated carbon (CCAC) for PFOA removal, with a maximum adsorption capacity of 34 mg/g, and recyclability of four regeneration cycles [69]. The DFB-linked polymer (DFB-CDP) achieved up to 99% PFOA removal at equilibrium, performing significantly better than when tetrafluoroterephthalonitrile (TFN) was used as the crosslinker to produce P-CDP (Figure 11a). Crosslinker chemistry was confirmed to be important for the efficient removal of PFAS, with the hydrophobic crosslinker DFB imparting hydrophobic characteristics to the β-CD polymer and improving PFAS removal for C4-C10 PFAS when compared to 2-isocyanatoethyl meth- acrylate (IEM) linked CDP and epichlorohydrin (EPI) linked CDP (Figure 11b) [70].
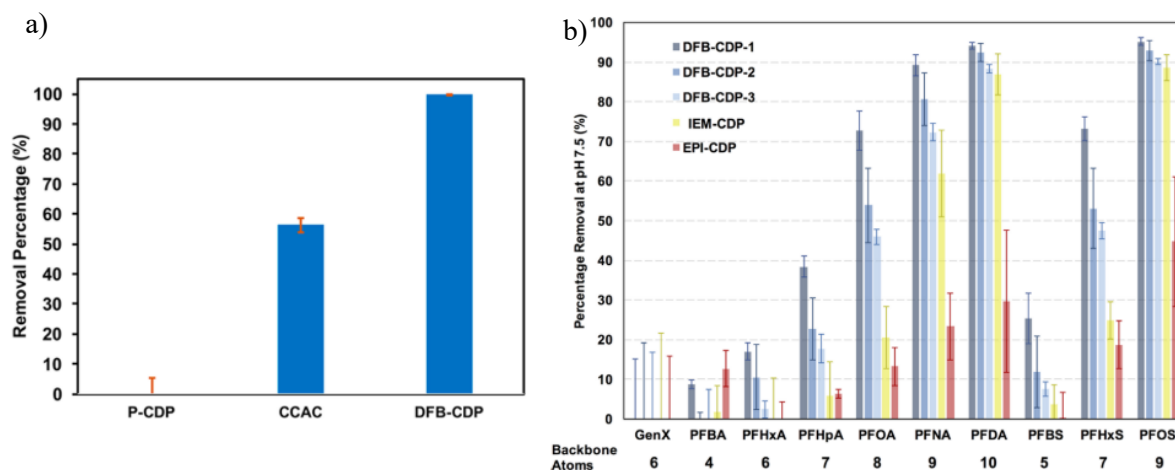
Figure 11: a) PFOA removal efficiency of P-CDP and DFB-CDP compared to commercial coconut shell activated carbon and b) PFAS removal efficiencies of DFB-CDP, IEM-CDP, and EPI-CDP. DFB-CDP 1-3 were prepared using increasing β-CD to DFB ratios. Figure a) from reference [69] and b) from reference [70].

24

2.6.3 Summary

As discussed in the preceding sections, several biomaterials are being investigated for PFAS removal from water, and adsorption capacities varying from the ng/g to the g/g range have been reported (Table 1). Due to the renewable nature of the base materials, and the recyclability of several adsorbents, they present promising alternatives to current PFAS removal techniques. However, despite the promise of the adsorbents, a need still exists to continue to innovate and search for adsorbents with facile synthesis methods that are efficient, renewable, economically feasible, and have a low environmental impact.

While cellulosic materials, such as fiber, cotton, and cellulose microcrystals have been studied for PFAS removal, no studies have yet focused on the use of CNCs as the base for a PFAS adsorbent. Since CNCs are abundant, renewable, nontoxic, and easily modified via physical and chemical processes, they offer an excellent basis for the development of novel PFAS adsorbents. CNC-based adsorbents for dyes and surfactants have been reported by Tam and co-workers [71], [72], [73]. Based on these studies, it was theorized that the application of CNC-based adsorbents can be further extended toward the removal of PFAS from water, which is the basis for the current study.

Table 1: Summary of maximum adsorption capacities of various adsorbents reported in the literature. Values reported were obtained at room temperature.

Sample	Adsorbent	PFAS	Maximum adsorption capacity (mg/g)	Reference
Lake water	Coal-based GAC	PFOA	0.52	[37]
Groundwater	Coal-based GAC	PFOA	1.1	[74]
		PFOS	5.3	
		PFHxS	0.6	
Groundwater	Coal-based PAC	PFOA	20	[74]
		PFOS	10	
		PFHxS	13	
PFAS solution	Resin	PFOS	207	[40]
Industrial wastewater	Bamboo-derived AC	PFOA	414	[51]
PFAS solution	Magnetic biochar	PFOA	204.7	[54]
		PFOS	195.5	
PFAS solution	Quaternized cotton	PFOA	1283	[63]
		PFOS	1650	
PFAS solution	Chitosan beads	PFOS	2500	[58]
PFAS solution	Chitosan-ethylene glycol hydrogel	PFOA	1200	[59]
PFAS solution	Starch-stabilized magnetic NPs	PFOA	62.5	[61]
Lake water	PEI-functionalized cellulose microcrystals	PFOA	2.32	[66]
PFAS solution	Functionalized CGF	PFOA	232.8	[65]
PFAS solution	β-CD-IL-MNPs	PFOA	2.5	[68]
		PFOS	13.5	
PFAS solution	β-CD polymer	PFOA	34	[69]

2.7 Material Selection for This Work

This section briefly outlines the materials selected for this study and explains the rationale behind the selections.

2.7.1 Cellulose Nanocrystals (CNCs)

Cellulose nanocrystals are a form of cellulose nanomaterial produced via the acid hydrolysis of cellulose fibers, typically from plant sources [75]. Cellulose fibers contain crystalline domains and amorphous regions. These amorphous regions are disintegrated during the acid hydrolysis process, resulting in the production of CNCs (Figure 12). CNCs produced from plant sources are typically 5-70 nm laterally and 100-250 nm in length. The acid used in the acid hydrolysis process determines the surface functional groups on the CNCs. CNCs have several properties that make them attractive for use in the development of adsorbent materials. CNCs are renewable, non-toxic, biodegradable, highly abundant, and have large surface areas
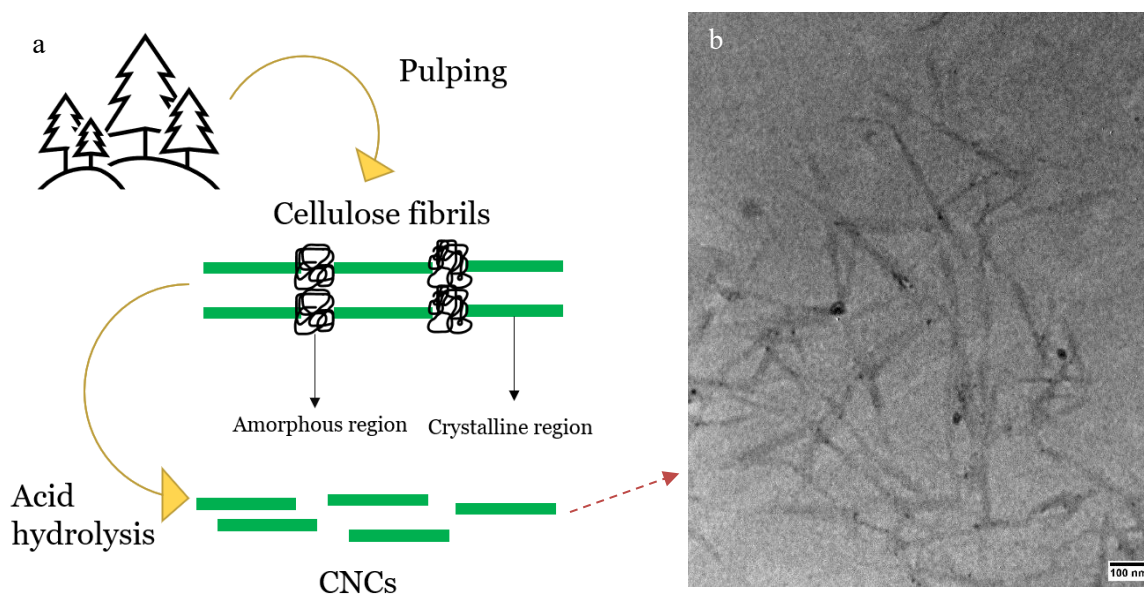
Figure 12: a) Schematic showing the process of CNC production from wood and b) TEM micrograph of pristine CNCs.

that provide many active sites for adsorption [76]. Furthermore, the abundance of hydroxyl groups on the CNC surface provides sites for surface modification through various chemical processes, making CNCs highly tunable (Figure 13).

In this study, CNCs were selected due to their high tunability, abundance, biocompatibility, and renewable nature. The CNCs used for the experiments described in this work have a negative surface charge due to the presence of sulfate groups, which allows for electrostatic interactions with the cationic coating material, Tanfloc, while the hydroxyl groups allow for the chemical modification of the CNCs to improve adsorptive properties.
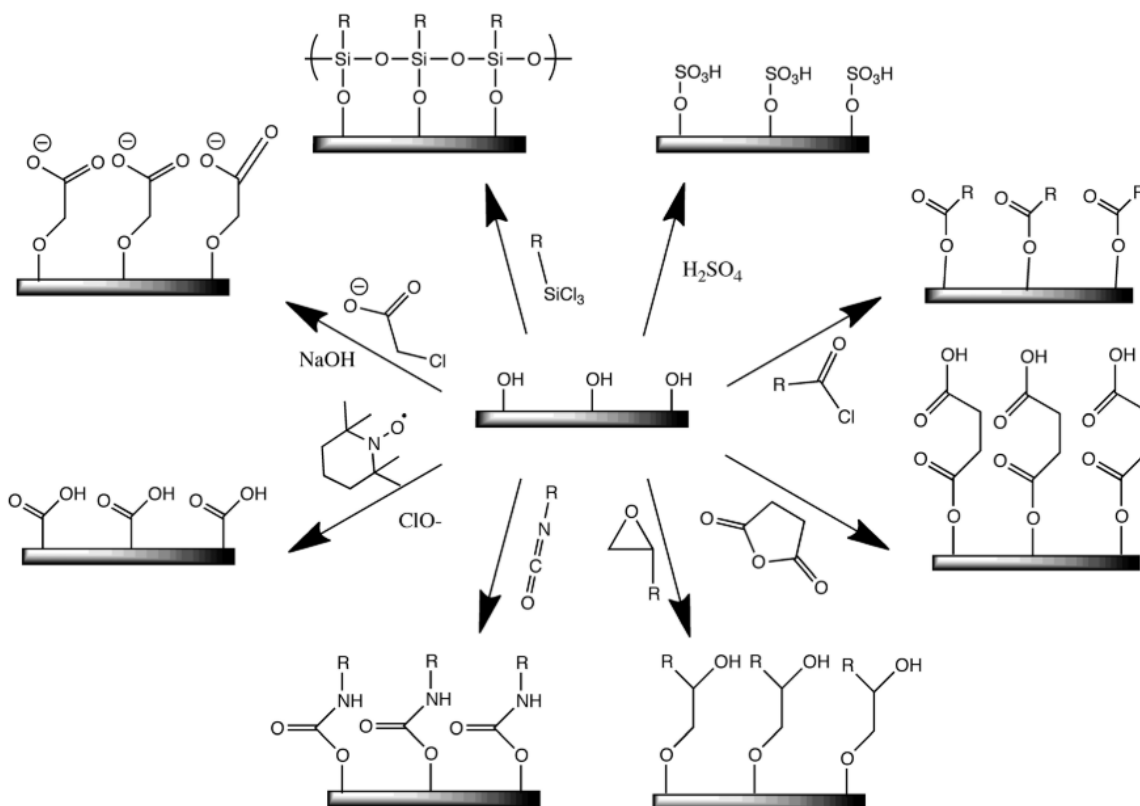
Figure 13: Common chemical modifications of CNCs. Figure adapted from reference [76].

Finally, CNCs have already been shown to adsorb contaminants such as the dyes methylene blue [77] and crystal violet [78], and heavy metal ions such as Ag(I), Cu(II), and

Fe(III) [79]. The adsorptive properties and tunability of CNCs could allow for the development of a multi-target adsorbent for the removal of several different contaminants from water.

2.7.2 Glycidyltrimethylammonium chloride (GTMAC)

GTMAC (Figure 14) is a cationizing agent that can be grafted onto hydroxyl groups via a ring-opening reaction. The cationization of CNCs with GTMAC has been reported previously, via semi-dry [80] and wet [81] processes. The highly positive surface charge after
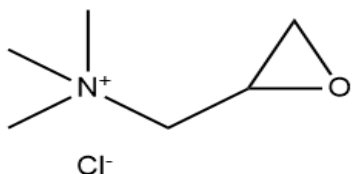
Figure 14: Chemical structure of GTMAC.

cationization with GTMAC could be used to encourage electrostatic interactions with anionic PFAS for water treatment, while the cellulose backbone provides sites for hydrophobic interactions with the carbon chain of target PFAS.

2.7.3 β-Cyclodextrin

Due to the rigid shape of the glucopyranose units that make up β-CD, β-CD molecules are shaped like truncated cones with an inner wide-end diameter of 7.8 Å [67]. The hydrophobic nature and size of the cavity allows β-CD molecules to form 1:1 and 2:1 host-guest interactions with PFAS such as PFOA [11]. The nature of the interaction depends on factors such as ionic strength and pH of the solution.

The ability of β-CD to capture PFAS molecules from water through hydrophobic interactions, its renewability and nontoxicity, and previous reports of CNCs grafted with β-CD [73], [82], led to the selection of this material for this study.

2.7.4 Tanfloc

Tanfloc (TN) (Figure 15) is a cationic, tannin-based polymer extracted from the black wattle tree (*Acacia mearnsii)*, and is used as a flocculant in water treatment [83]. Since tannin-based materials are biodegradable, non-toxic, and derived from plants, they are excellent for the development of more sustainable technologies. The positive charge in TF is derived from substituted amine groups, and TN has been reported to form polyelectrolyte complexes with alginate, an anionic polysaccharide [84]. Its sustainability, cationic nature, and its ability to complex with anionic polymers make Tanfloc an excellent candidate to prepare CNCs with a positive surface charge without requiring chemical modification.
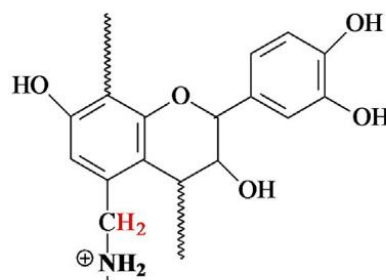
Figure 15: Theoretical structure of Tanfloc. Figure adapted from reference [83].

2.7.5 Sodium Alginate

Sodium alginate (AG) is an anionic polysaccharide found in brown algae and its basic structure consists of linear copolymers of 1 → 4 linked *α-D*-mannuronic acid and *β-L*-guluronic acid [85]. Alginate can interact with divalent cations such as calcium to produce thermally stable and biocompatible hydrogel beads, which are widely used to encapsulate microbial cells, enzymes, hormones, drugs, and oils. CNC-AG hydrogel beads containing anionic CNCs have previously been reported as adsorbents for organic dyes in aqueous solutions [71], [72], as have hydrogels produced from cationic CNCs and AG [86]. AG was selected for this study due to its ability to form hydrogel beads with CNCs, which can then be employed as sustainable and biodegradable adsorbents for PFAS removal from water.

30

2.7.6 Summary

This section discusses the materials selected for the development of nanocellulose-based PFAS removal systems. CNCs, β-CD, Tanfloc, and AG were all selected for their biocompatibility, biodegradability, and natural origins. Tanfloc and GTMAC were selected for their ability to impart a cationic charge to the CNCs to allow for electrostatic interactions with anionic PFAS present in water, while β-CD was selected for its potential for hydrophobic host-guest interactions with PFAS. Finally, AG was selected for its ability to produce stable hydrogel beads with CNCs in the presence of calcium cations, allowing for the production of adsorbent beads that can be utilized in water treatment systems such as column filters.

Chapter 3: Chemically Modified CNCs and their Adsorptive Properties

3.1 Introduction

The prevalence of PFAS in different water sources is of growing concern due to the bioaccumulation of these highly stable compounds [19], [20], [24], which can lead to health problems such as diabetes, reduced kidney function, and inflammation [87], [88], [89], [90]. While modified cellulose has been studied for PFAS removal from water [63], [65], [66], few studies have been reported on chemically modified nanocellulose for PFAS removal.

In this study, CNCs were selected as a nano-template for the development of adsorbents for water treatment because they are naturally sourced and have an abundance of hydroxyl groups that can be chemically modified. Cationized CNCs were synthesized using GTMAC as the cationizing agent, while CNCs that would promote hydrophobic and host-guest interactions with PFAS were synthesized by grafting β-CD onto CNCs. The synthesized materials were characterized, and used as the adsorbent to remove methyl orange (MO) and KPFBS and determine the adsorption efficiency of the synthesized materials.

3.2 Experimental Procedure

3.2.1 Materials

Cellulose nanocrystals (5-20 nm width and 100-200 nm length) were donated by CelluForce Inc. Glycidyltrimethylammonium chloride (GTMAC) solution, β-CD, sodium hydroxide (NaOH) pellets, epichlorohydrin (EPI), phenolphthalein ($C_{20}H_{14}O_4$) (Phe) powder, silver nitrate ($AgNO_3$) powder, methyl orange (MO), potassium bromide (KBr), potassium chloride (KCl), and dimethylsulfoxide (DMSO) were purchased from Sigma-Aldrich and used as received. Ethanol was purchased from Fisher Scientific. Potassium perfluorobutanesulfonate (KPFBS) was purchased from the Tokyo Chemical Industry (TCI)

and used as received. Milli-Q water (resistance $\geq$ 18 MΩ/cm) was generated by a Millipore Mill-A purification system.

3.2.2 Cationization of CNCs with GTMAC

The cationization of CNCs was performed using a semi-dry procedure adapted from the procedure reported previously by Zaman et. al [80]. 1 g of powdered CNCs and 50 mg of NaOH pellets were mixed thoroughly with a mortar and pestle, which caused the temperature of the mixture to rise. The mixture was allowed to cool to room temperature and transferred to a resealable polyethylene bag. The solvent was then added to the mixture (Milli-Q water or a Milli-Q water/DMSO system). The mixture was kneaded by hand, and GTMAC (3:1 molar ratio of GTMAC to anhydroglucose units) was added dropwise to the mixture. The mixture was kneaded as the GTMAC was added. Following the addition of GTMAC, the mixture was placed in an ultrasonic bath at 60 °C for 6 hours. The reaction was stopped by precipitation in ethanol, and the unreacted reagents and by-products were removed through centrifugation. The pellet was redispersed in water and placed in a Labconco freeze dryer to remove the water over 72 hours. The dried cationized CNC (GCNC) powder obtained after freeze drying was stored at ambient conditions.

3.2.3 Synthesis of β-CD Grafted CNCs

β-CD grafted CNCs (β-CD-CNC) were synthesized following a procedure adapted from Lin and Dufresne [82]. 20 g of β-CD was first dissolved in 40 mL of 5 M NaOH. 2 g of CNC was dispersed in 40 mL of Milli-Q water and added to the β-CD solution and stabilized for 30 minutes at room temperature. Following this, 11.92 mL of EPI was added dropwise to the

solution under vigorous stirring. The reaction was allowed to proceed at 40 °C for 6 hours. After modification, the suspension was centrifuged at 8500 rpm for 1 hour. The supernatant was removed, and the pellet was redispersed, washed, and repeatedly centrifuged until neutrality to remove ungrafted β-CD and residual NaOH. Finally, the material was freeze-dried for 3 days and a powder was obtained. The powdered β-CD-CNC was stored at ambient conditions.

3.2.4 Batch Adsorption Experiments

To test the adsorptive performance of the synthesized materials, batch adsorption experiments were conducted as described in the following sections.

3.2.4.1 Adsorption of MO by GCNC

MO solutions with composition 50, 100, 500, and 1000 ppm were prepared in Milli-Q water, followed by the addition of 30 mg of powdered, freeze-dried GCNC to 5 mL of dye solution (adsorbent concentration of 6 mg/mL). The resulting dispersions were allowed to equilibrate on a shaker overnight. The solutions were then centrifuged to remove the dispersed GCNC. UV-vis measurements were conducted at 464 nm with a Cary 100 Bio UV-vis spectrophotometer to determine the concentration of MO remaining in the supernatant.

3.2.4.2 Adsorption of MO by β-CD-CNC

MO solutions of composition 5, 10, 20, 50, 100, 200, 400, 500, 1000, and 2500 ppm were prepared in Milli Q water, and 100 mg of powdered, freeze-dried β-CD-CNC was added to 5 mL of each solution (β-CD concentration of 2.5 mg/mL). The solutions were allowed to equilibrate overnight on a shaker. The solutions were filtered to remove the β-CD-CNC and

UV-vis measurements were conducted at 464 nm with a Cary 100 Bio UV-vis spectrophotometer to determine the remaining MO in solution.

3.2.4.3 Adsorption of KPFBS

40 mL of 250 µM KPFBS solutions were prepared in 10 mM KCl. GCNC (325 mg) and β-CD (439 mg) were added in powder form to various solutions. These solutions were allowed to equilibrate overnight on a shaker. After adsorption, the adsorbent was removed from the solution via ultrafiltration through a 0.1 µm membrane. The KPFBS concentration of the filtrate was measured using an ion-selective electrode (ISE) for KPFBS. To reduce signal drift between measurements, a new sensor tip with a fresh membrane was used for each sample.

3.3 Material Characterization

3.3.1 Hydrodynamic Size and Zeta Potential Measurements

The zeta potential (ZP) of the GCNC was determined using a Malvern Nano-ZS90 Zetasizer. Samples were prepared by diluting purified GCNC solution to 0.1% (w/w) in Milli-Q water. Samples were sonicated using a probe sonicator for 2 minutes before measurements were conducted. ZP measurements were based on electrophoretic potential at room temperature. All measurements were repeated three times and data are presented as averages of three measurements.

3.3.2 Quantification of Quaternary Ammonium Groups in GCNC

The amount of quaternary ammonium groups incorporated in the GCNC was determined via potentiometric titration with silver nitrate using a Metrohm Titrando system coupled with a Ag/AgCl reference electrode. Silver nitrate undergoes a displacement reaction with chloride

ions to form insoluble silver chloride, resulting in increasing solution turbidity and decreasing the number of free ions in solution, which results in a change of the EMF of the system [91]. The volume of titrant used to reach the endpoint of the titration is used to calculate the moles of silver, which is equivalent to the moles of chloride ions and quaternary groups present in the sample solution. GCNC sample solution (20-25 mL, 1 mg/mL) was titrated with 10 mM AgNO$_3$ solution, and the amount of GTMAC in each sample was calculated using the equation:

$$mol_{GTMAC} = V_T \times C_T \tag{Eq. 5}$$

where mol_{GTMAC} is the moles of GTMAC in the sample, V_T is the total volume of titrant added at the endpoint, and C_T is the concentration of the titrant. The percentage of GTMAC grafted on CNC was then calculated using the equation:

$$\%GTMAC\ grafted = \frac{mol_{GTMAC}}{mol_{OH}} \times 100\% \tag{Eq. 6}$$

where mol_{OH} is the number of potential grafting sites present in the sample solution. Lower and upper bounds of grafting percentage were calculated based on the minimum and maximum number of free hydroxyl groups present in each repeating unit.

3.3.3 Fourier Transform Infrared Spectroscopy (FTIR) of β-CD-CNC

FT-IR spectroscopy was conducted using a PerkinElmer 1720 FT-IR spectrometer to validate CNC modification. Samples were prepared by grinding them with KBr and using a hydraulic press to form transparent pellets. The pellets were scanned using the spectrometer at a resolution of 4 cm^{-1} to obtain the spectra.

3.3.4 Determination of β-CD Content in β-CD-CNC

The amount of β-CD grafted onto CNC was measured using a phenolphthalein (Phe) indicator test. A standard curve relating the amount of β-CD to Phe absorbance was generated using UV-visible spectrophotometry, and the amount of β-CD present in the β-CD-CNC was determined using the standard calibration curve. Samples and standards were prepared as follows: 2 mL of a 0.1% (w/v) Phe solution in 1:1 ethanol to water was added to a 50 mL centrifuge tube, followed by 2 mL of 0.005 M NaOH. For the standard curves, 0-10 mL of a 1 mg/mL β-CD solution were added to the base-indicator solution, and the final solution volume was adjusted to 25 mL with the addition of Milli-Q water. For sample solutions, 100 mg of powdered β-CD-CNC was added to the base-indicator solution, and the final solution volume was adjusted to 25 mL. The samples were placed on a shaker overnight and filtered through filter paper prior to UV-vis measurements. Absorbance was measured at 464 nm, and the amount of β-CD present in each sample was calculated using the standard curve. The β-CD content was calculated using the equation:

$$\% \beta - CD \; grafted = \frac{mass_{\beta-CD}}{mass_{CNC}} \times 100\% \qquad \text{(Eq. 7)}$$

Lower and upper bounds of grafting percentage were calculated based on the minimum and maximum number of free hydroxyl groups present in each repeating unit.

3.4 Results and Discussion

3.4.1 Synthesis and characterization of GCNC
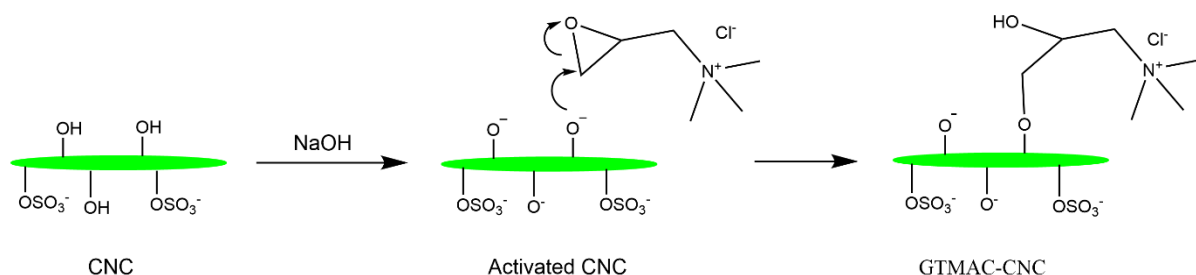
Figure 16: Modification of CNC with GTMAC to prepare cationic CNCs.

GCNC was synthesized through a ring opening reaction between the deprotonated hydroxyl groups in CNCs and the three-membered ring in GTMAC (Figure 16). To determine the effect of the solvent system on grafting efficiency, the semi-dry process was conducted with water as the sole solvent and with a 2:1 DMSO:water solvent system. Zeta potential results (Figure 17) show an increase in the zeta potential from -37.8 ± 3.7 mV to +48.4 ± 1.5 mV for the GCNC synthesized with water as the solvent. There was a slightly larger increase in the zeta potential to +52.1 ± 2.1 mV in the GCNC synthesized using DMSO and water as the solvent system. The charge reversal of CNCs from negative to positive confirmed the grafting of GCNC onto the CNC surface, and agreed with similar changes reported in the literature [80], [81].
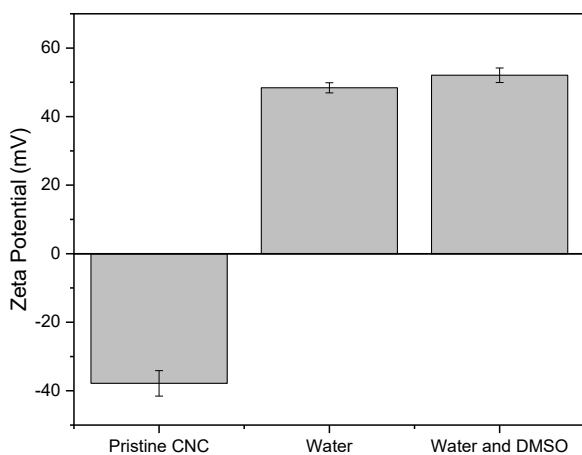
Figure 17: The zeta potential of pristine CNCs and GCNC prepared using the semi dry process using different solvent systems.

To determine the grafting efficiency of GTMAC onto the CNCs, a conductometric

titration with silver nitrate was conducted. The volume of silver nitrate required to neutralize the chloride counterions present in the sample solutions was determined from titration curves such as one shown in Figure 18a. The titrant volume was then used to calculate the grafting
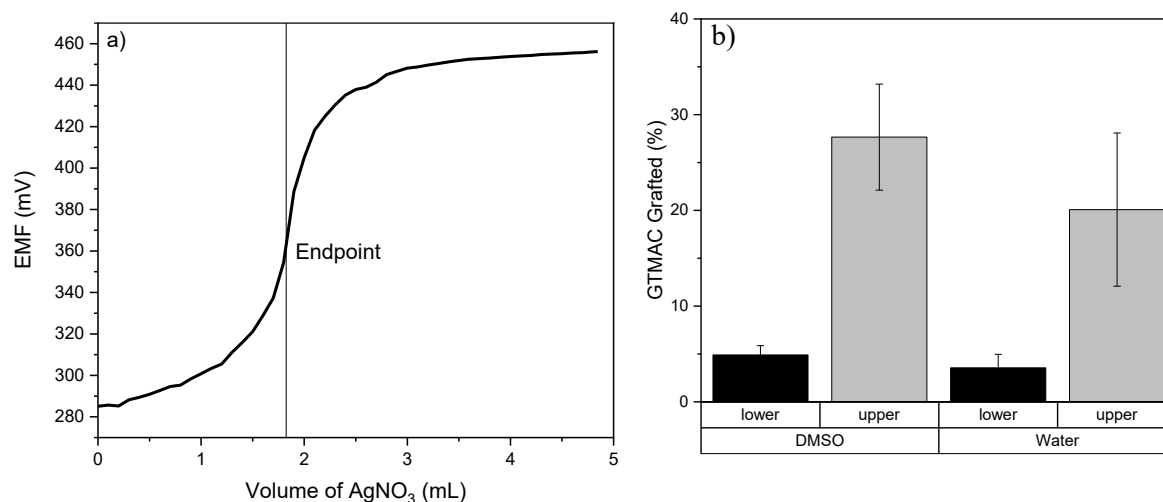
Figure 18: a) A representative titration curve generated from a silver nitrate titration to determine the grafting efficiency of GTMAC onto CNCs and b) the upper and lower bounds of percent GTMAC grafting in water and water + DMSO as the solvent.

efficiency using Equations 5 and 6. The theoretical ranges in which grafting efficiency falls are shown in Figure 18b. The upper and lower bounds were calculated by assuming 1 and 3 grafting sites available on each anhydroglucose unit in CNC, and of those, 1 and 3 sites modified. The combined use of DMSO and water as co-solvents led to higher grafting efficiencies (5-28%) than that achieved with water alone (4-20%). The decrease in grafting efficiency when using water as the sole solvent is due to the hydrolysis of epoxide groups in water, which reduces the number of GTMAC molecules available to react with the CNCs [80]. Another reason for the reduction in grafting is the salting out of GTMAC as the sodium chloride concentration increased in solution as the reaction proceeded and released chloride

ions into the solution [92]. However, since only a small volume of water (2 mL) was used for the reaction, the salting out effect was unlikely to have been significant.

Finally, the quaternization of CNCs was further validated through FT-IR spectroscopy. The FT-IR spectra (Figure 19) of the GCNC prepared in water and in the DMSO/water system both showed the appearance of a prominent band at 1479 cm^{-1}, which corresponds to the methyl groups of the GTMAC [80].
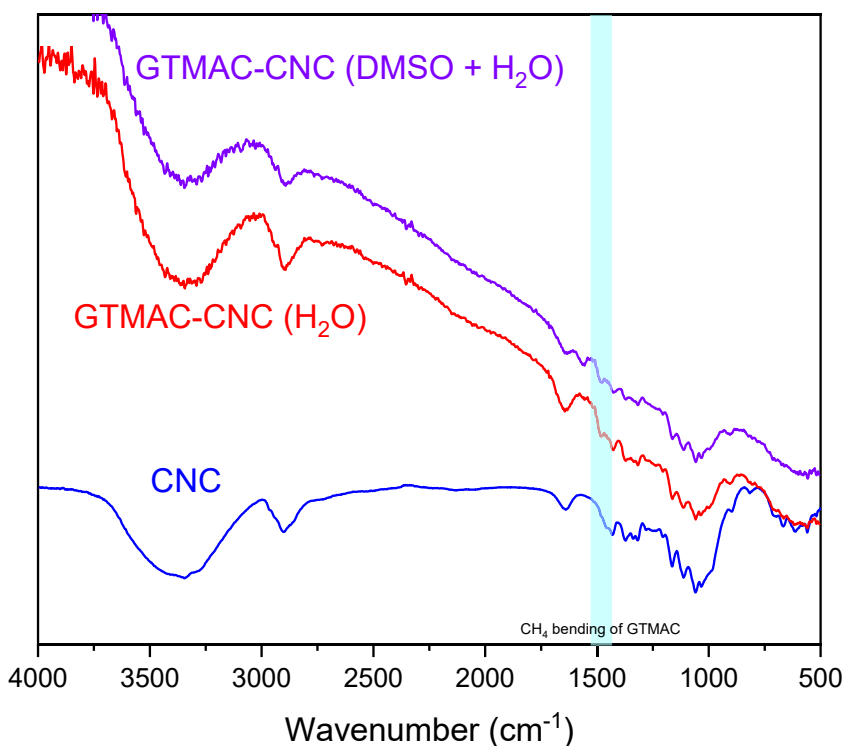
Figure 19: FT-IR spectra of pristine CNC, and GCNC prepared in water and DMSO/water.

3.4.2 Synthesis and characterization of β-CD-CNC

β-CD-CNC was synthesized using EPI as the crosslinker to connect the hydroxyl groups on CNCs with β-CD (Figure 20). The addition of base deprotonated the hydroxyl groups and

allowed them to participate in nucleophilic substitution and ring opening reactions with EPI, resulting in β-CD grafting onto CNCs. To prevent the self-crosslinking of β-CD, the EPI/β-CD
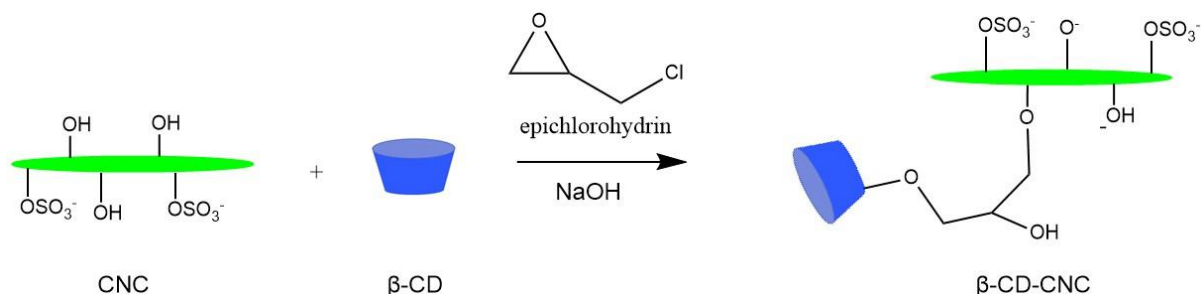
Figure 20: Reaction scheme for the synthesis of β-CD-CNC.

ratio was kept below 10 [82].

The grafted β-CD content in the β-CD-CNC was determined using UV-vis spectrophotometry, with phenolphthalein (Phe) as the indicator. In the presence of β-CD, the pink Phe solution loses its colorimetric intensity due to the formation of a β-CD-Phe complex [93]. The corresponding reduction (Figure 21a) in UV-vis absorbance can be used to determine the amount of β-CD present in a sample. A calibration curve relating the mass of β-CD to
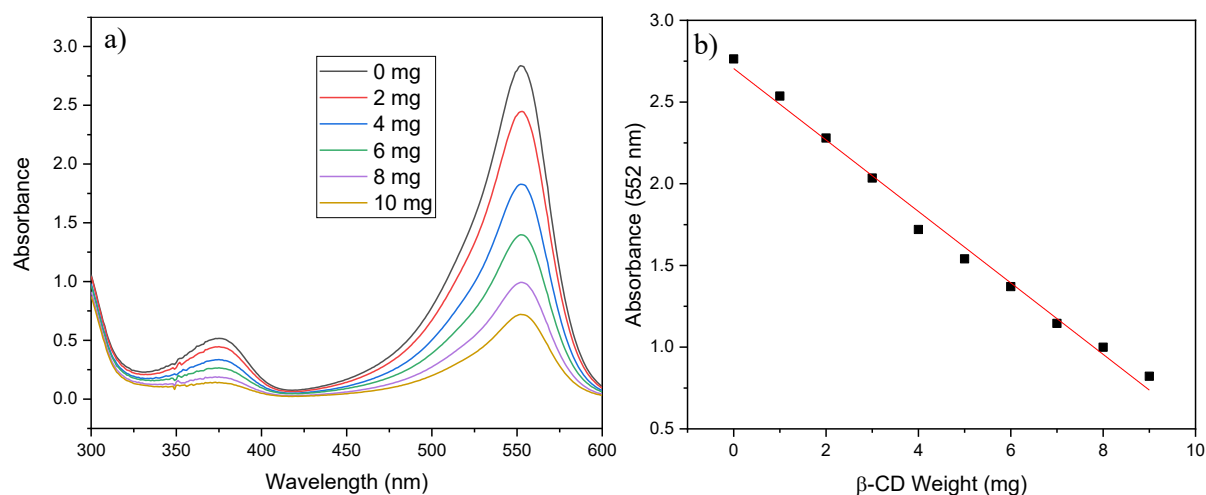
Figure 21: a) UV-vis spectra of β-CD in Phe solution, and b) the calibration curve for the determination of β-CD using the Phe indicator assay (R^2 = 0.99034), equation: y = 2.70502 + - 0.21864x.

absorbance at 552 nm was constructed (Figure 21b) and the equation y = 2.70502 - 0.21864x was used to calculate the β-CD content of the β-CD-CNC (12.5% ± 0.9%).

FT-IR spectroscopy was used to further validate the successful grafting of β-CD onto CNC. After grafting β-CD onto the CNC, the intensities of the peaks found at 2912 cm^{-1} (C-H
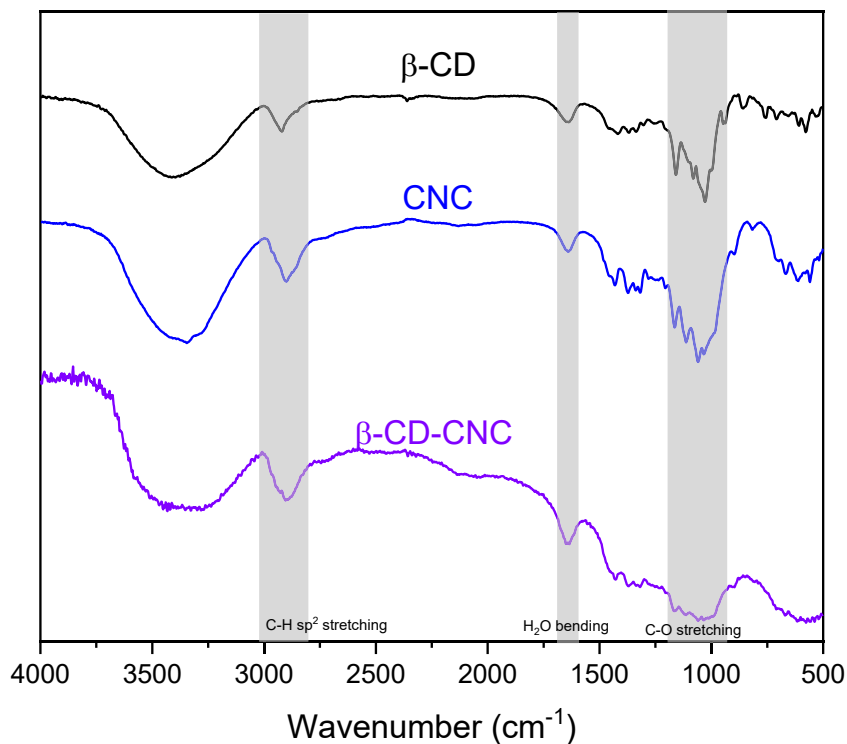
Figure 22: FT-IR spectra of β-CD, pristine CNC, and β-CD-CNC.

stretching) and 1645 cm^{-1} (O-H bending vibration) increased slightly, while there was a decrease in the peak intensity in the 1200 cm^{-1} to 950 cm^{-1} region. The peaks located in this region include the antisymmetric bridge oxygen stretching at 1163 cm^{-1}, antisymmetric in-phase ring stretching at 1113 cm^{-1}, and C-O stretching for cellulose at 1059 cm^{-1}. The increase in the peak intensity for the C-H stretching indicated the presence of additional C-H bonds of grafted β-CD, while the increase in O-H bending indicated water molecules present in the β-CD cavities [94]. The decrease in peak intensity in the 1200 cm^{-1} to 950 cm^{-1} region suggested

43

the formation of C-O bonds between the EPI and cellulose, and agreed with similar changes reported in the literature [82].

3.4.3 Adsorptive Performance of GCNC and β-CD-CNC

3.4.3.1 Adsorption of MO by GCNC

The adsorption of MO onto GCNC adsorbent led to an increase in dye removal as the initial dye concentration rose. The result was visually evident by the appearance of the pellet after centrifugation. The pellets obtained by centrifuging the sample with the initial MO concentrations of 500 ppm and 1000 ppm were much larger and bright orange in colour, while the pellets obtained from the 50 ppm and 100 ppm samples were slightly orange and did not contain large amounts of dye (Figure 23).

Figure 23: Pellets obtained after centrifugation of MO samples with GCNC as the adsorbent.

The increasing dye removal was confirmed through UV-vis spectroscopy. The UV absorbance of MO at 464 nm increased with increasing dye concentration (Figure 24a), and this trend was used to generate a MO calibration curve (Figure 24b). The calibration curve was used to determine the equilibrium concentration (C_e) of MO using the equation:
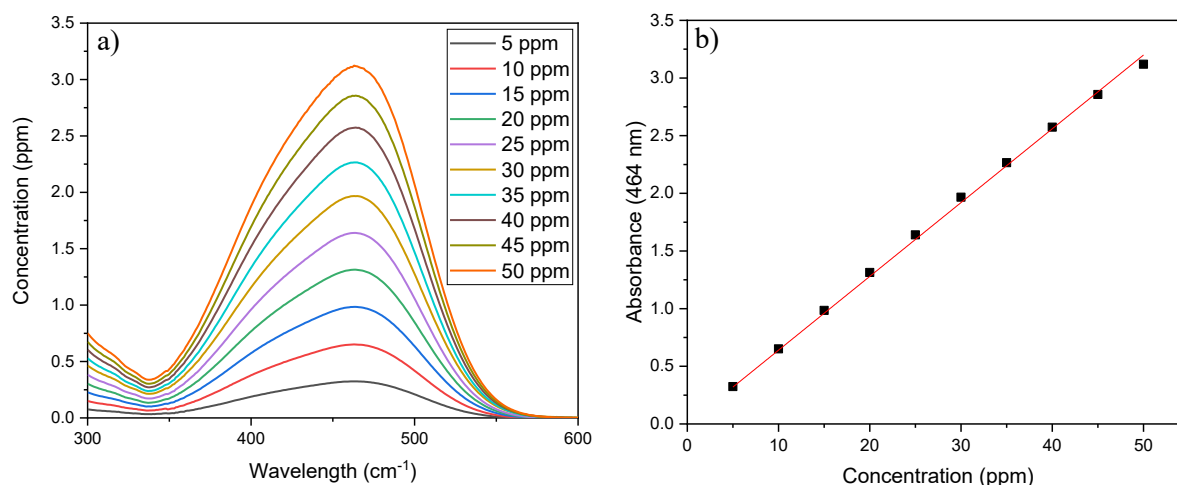
Figure 24: a) UV-vis spectra of increasing MO concentration and b) UV-vis calibration curve for MO. Equation: y = 0.06399x, R² = 0.99962.

$$C_e = \frac{Abs}{0.06399} \cdot dil \tag{Eq. 8}$$

where Abs is the UV absorbance at 464 nm and *dil* refers to the dilution factor used to prepare the sample for the measurement. C_e was then used to calculate the amount of dye adsorbed at equilibrium per gram of adsorbent (q_e) using the equation:

$$q_e = \frac{(C_b - C_e)\,(V_s)}{m_{ads}} \tag{Eq. 9}$$

where C_b is the bulk dye concentration, V_L is the sample volume, and m_{ads} is the mass of adsorbent added to the dye sample.

A plot of q_e against C_e revealed an increase in the amount of dye adsorbed with increasing dye concentration at equilibrium (Figure 25a), which corresponded to increasing initial concentrations of dye. The increase in adsorption capacity with the increase in the MO concentration was also supported by the increase in removal efficiency as the dye concentration increased, with 9.5% removal at 50 ppm MO and 80% removal at 1000 ppm (Figure 25b).

45
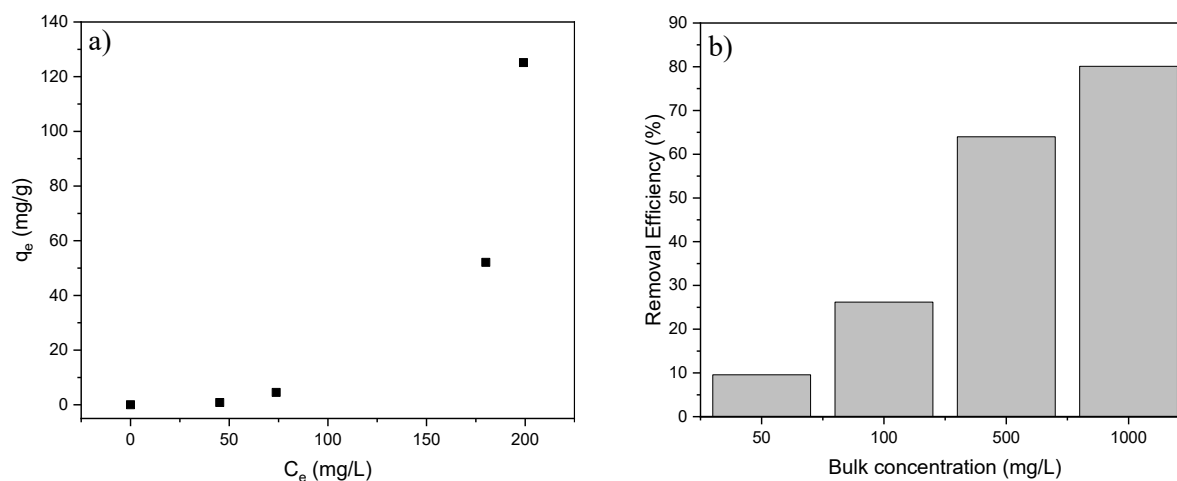
Figure 25: a) Equilibrium adsorption data of GCNC as the solvent with 0, 50, 100, 500, and 1000 ppm of MO as the starting concentrations, and b) percent removal of MO by 30 mg of GCNC as the adsorbent.

Generally, an increase in initial dye concentration results in the saturation of adsorption sites and leads to an eventual decrease in removal efficiency [95]. However, in some cases, an increase in initial dye concentration may lead to an increase in the dye loading capacity of the adsorbent [96]. This increase may be due to an excess of adsorption sites present in the solution, which were not saturated by the dye molecules present. The increase may also be due to stacking interactions between MO molecules, which would increase with an increase in dye concentration and result in greater removal. To determine the saturation point of GCNC and determine maximum adsorption loading capacity, adsorption should be conducted at higher MO concentrations or lower adsorbent amounts. The high MO removal efficiencies of GCNC at high initial dye concentrations indicated that this adsorbent may be more suitable for the remediation of samples containing high contaminant concentrations, such as industrial wastewater.

3.4.3.2 Adsorption of MO by β-CD-CNC

Treatment of MO with β-CD-CNC resulted in dye uptake by the powdered adsorbent. Since the adsorbent did not disperse in the dye solution, the solid adsorbent settled to the bottom of the sample vials after being removed from the shaker, with a clear supernatant visible above the spent adsorbent (Figure 26).
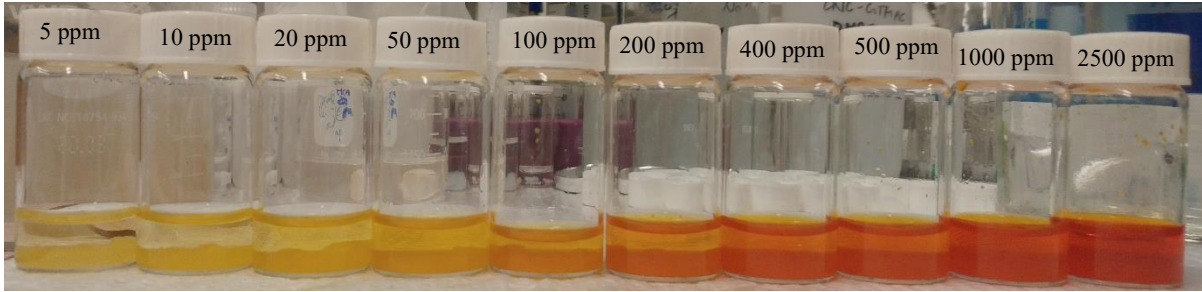
Figure 26: MO solutions after being treated with β-CD-CNC as the adsorbent.

The experimental data from UV-vis spectroscopic analysis of the supernatants were then utilized in Equations 8 and 9 to obtain C_e and q_e for the samples. The resulting plot of q_e against C_e was fitted to the Langmuir and Freundlich isotherms (Figure 27a) using non-linear curve fitting in Origin 2018. The Langmuir and Freundlich isotherms are respectively described by Equations 10 and 11:

$$q_e = \frac{q_m K_L C_e}{(1 + K_L C_e)} \tag{Eq. 10}$$

$$q_e = K_F (C_e)^{1/n} \tag{Eq. 11}$$

where K_L is the Langmuir constant (L/mg) and q_m is the theoretical maximum adsorption capacity of the adsorbent in mg/g. K_F, also known as the Freundlich constant, describes adsorbate loading on the adsorbent (units of $(mg/g)(L/mg)^{1/n}$), and $1/n$ is related to the heterogeneity of the adsorbent surface. From the fitted data, the predicted values of K_L and q_m were 0.56 L/g and 125.7 mg/g, respectively. K_F and n were 0.24 $(mg/g)(L/mg)^{1/n}$ and 1.3,

respectively. Since the experiments were limited by MO solubility and did not reach saturation, the obtained parameters must be interpreted with caution. Adsorption tests with reduced adsorbent mass should be conducted to determine experimental parameters and the validity of the predicted parameters.

Both isotherms showed good fitting to the data, with the Freundlich isotherm showing a slightly better fit with a sum of squared error (SSE) of 3.4 compared to an SSE of 5.6 for the Langmuir isotherm. The similar SSE and R^2 values (0.99778 for Langmuir and 0.99864 for Freundlich) suggest that the adsorption of MO by β-CD-CNC could be described well by both models.

The removal efficiency of MO ranged from 44% at an initial dye concentration of 2500 ppm to 71% at an initial dye concentration of 20 ppm (Figure 27b). The removal efficiency data suggest that β-CD-CNC may be more suitable for contaminant removal at concentrations
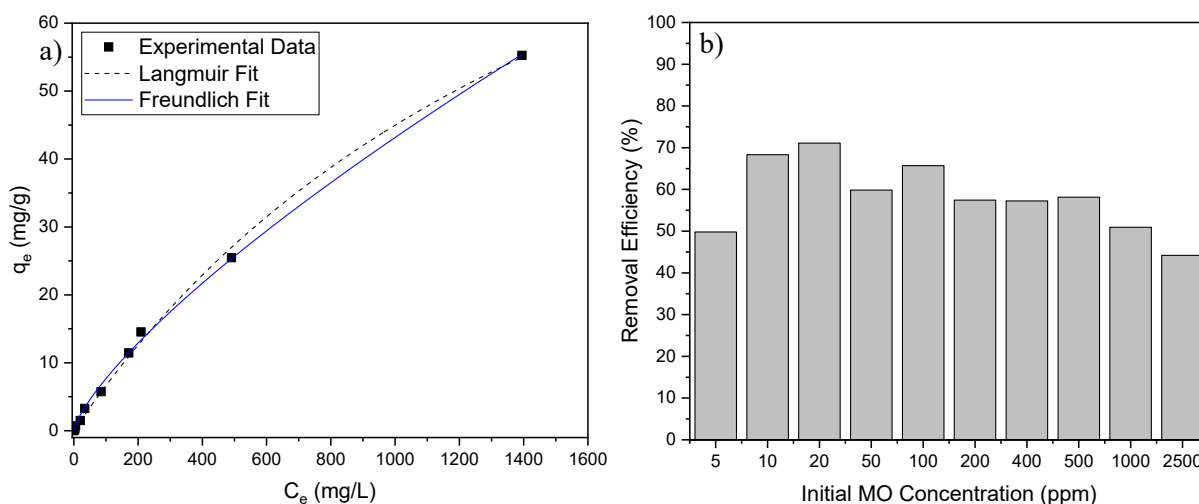
Figure 27: a) Adsorption isotherm of MO adsorption onto β-CD-CNC and b) removal efficiency of MO by β-CD-CNC.

48

between 10 and 100 ppm. However, the adsorbent may still be effective between 100 and 1000 ppm, as it achieved between 50-58% removal at these concentrations.

3.4.3.3 Adsorption of KPFBS

The treatment of 250 μM KPFBS with GCNC and β-CD-CNC resulted in removal efficiencies of 43.7 and 56.5%, respectively (Figure 28). The removal of KFPBS by GCNC was greater than the removal of MO by GCNC, while the removal of KPFBS by β-CD-CNC was lower than the removal of MO by β-CD-CNC. This may be due to the varying degree of electrostatic and hydrophobic interactions in the two systems. These results indicate that GCNC and β-CD-CNC are promising adsorbents for the removal of short-chain PFAS, such as PFBS. However, it is important to note that the ISE system used to calculate KPFBS concentrations is still in its preliminary stages, and this method of measurement is not the standard for PFAS quantification. To validate these results, KPFBS should be quantified using the standard analytical methods of high-performance liquid chromatography (HPLC) and mass spectrometry.
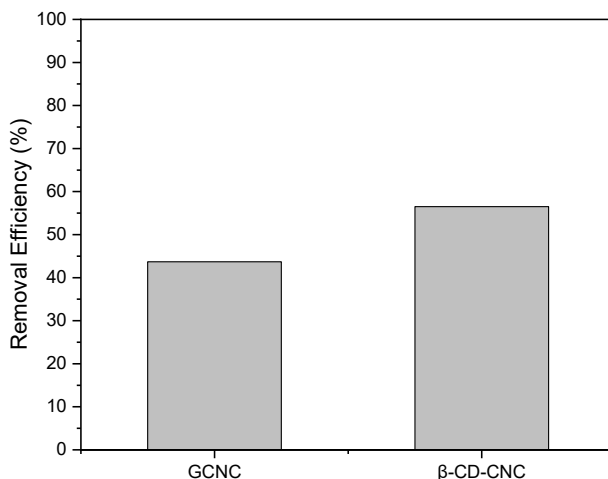
Figure 28: Removal of KPFBS by GCNC and β-CD-CNC. Initial concentration of KPFBS = 250 μM in 10 mM KCl.

3.5 Conclusions

This chapter presents the synthesis, characterization, and adsorptive properties of chemically modified CNCs. CNCs were successfully cationized with GTMAC to generate GCNC. The grafting reaction conducted in a 2:1 DMSO/water solvent system resulted in up to 28% GTMAC grafting and produced highly stable cationic CNCs with a zeta potential of +52.1 ± 2.1 mV. The GCNC achieved between 9.5% and 80% MO removal, with higher removal efficiencies at higher initial dye concentrations, suggesting that this adsorbent is suitable for wastewater samples with high concentrations of anionic contaminants. GCNC achieved 43.7% removal of KPFBS from a laboratory sample, suggesting that this adsorbent may be used to enhance short-chain PFAS removal from water.

β-CD-CNC with 12.5% ± 0.9% β-CD content was synthesized to generate an adsorbent for removing contaminants through hydrophobic host-guest interactions. Batch adsorption tests showed good fitting with both the Langmuir and Freundlich isotherms. The theoretical maximum adsorption capacity of the adsorbent was determined to be 125.7 mg/g, and the adsorbent achieved up to 71% MO removal at an initial dye concentration of 20 ppm, suggesting that this adsorbent is suitable for the removal of anionic contaminants at low initial concentrations. The adsorbent also achieved 56.5% removal of KPFBS from water, suggesting that β-CD-CNC is a promising adsorbent for the removal of short-chain PFAS from water.

Chapter 4: Coated CNCs and their Adsorptive Properties

4.1 Introduction

Current methods of PFAS remediation, such as GAC, RO, and NF have large financial and environmental costs associated with them [8]. Due to these drawbacks, the development of low-cost, environmentally friendly adsorbents is desirable. The simplest method for the generation of these adsorbents is one that does not require large amounts of organic solvents and chemicals and does not involve multiple synthesis steps. Electrostatic interactions between oppositely charged particles to form polyelectrolyte complexes (PEC) offer a facile method to prepare charged particles [97]. Since the PEC particles carry a surface charge, they can be utilized as adsorbents to attract target contaminants with the opposing charge.

CNCs prepared through sulfuric acid hydrolysis carry a negative surface charge due to the presence of sulfate groups [98]. The negative charge can be utilized to coat the CNCs with positively charged polymers such as chitosan [99] and lignin [100] to produce CNC-based complexes with a positive surface charge. The coating process is simple and green, as it involves the mixing of the oppositely charged materials without the use of any harsh chemicals.

This chapter describes the coating of CNCs with the positively charged, lignin-based, commercially available flocculant, Tanfloc. The surface charge of two types of Tanfloc, Tanfloc SH (TFSH) and Tanfloc SG (TFSG) was studied over a range of pH values, and the optimal conditions for the preparation of Tanfloc-coated CNCs (TFSH-CNC and TFSG-CNC) were determined. The prepared material was crosslinked with sodium alginate to produce hydrogel beads, and the adsorptive properties of the beads were studied using MO and KPFBS.

4.2 Experimental Procedures

4.2.1 Materials

Cellulose nanocrystals (5-20 nm width and 100-200 nm length) were donated by CelluForce Inc. Tanfloc SG and Tanfloc SH were donated by Tanac, Brazil. Both types of Tanfloc are lignin-based, cationic polymers [101]. Tanfloc SH has been modified to have a higher molecular weight than SG, with the other chemical and physical properties being the same as presented on the MSDS for each chemical. Sodium alginate (ALG), calcium chloride dihydrate ($CaCl_2.2H_2O$), potassium bromide (KBr), potassium chloride (KCl), and methyl orange (MO) were purchased from Sigma Aldrich and used as received. Potassium perfluorobutanesulfonate (KPFBS) was purchased from the Tokyo Chemical Industry (TCI) and used as received. Milli-Q water (resistance $\geq$ 18 MΩ/cm) was generated by a Millipore Mill-A purification system.

4.2.2 Preparation of TF-CNC

To prepare TF-CNC, powdered CNCs were dispersed in Milli-Q water to yield a 2% CNC dispersion. TF was added to an equivalent volume of water and stirred until dissolved. The TF solution was slowly added to the CNC dispersion while stirring. Following the addition of TF, the mixture was homogenized using an IKA homogenizer. The homogenized mixture was stirred and centrifuged at 8500 rpm for 60 minutes to remove excess TF. The pellet was redispersed in Milli-Q water and freeze-dried for 2 days to yield powdered TF-CNC.

For the experiments aimed at optimizing coating composition, the TF:CNC ratio was varied from 0.5:1 to 3:1. For preparation time optimization, a constant ratio of 3:1 TF:CNC was used and the mixtures were stirred for 0 to 5 days.

4.2.3 Preparation of Hydrogel Beads

To prepare hydrogel beads, 4-8% w/w dispersions of TF-CNC were prepared in Milli-Q water. The TF-CNC dispersions were homogenized and added to a 1% solution of sodium alginate. The TF-CNC-ALG mixture was homogenized once again and added dropwise with a 14-gauge needle to the gelation bath (1L, 180 mM $CaCl_2.2H_2O$). The beads were allowed to crosslink for 30 minutes in the gelation bath while being gently stirred to prevent clumping. After crosslinking, the beads were removed from the gelation bath using a nylon mesh and dialyzed against DI water for 2 days to remove excess calcium chloride. After dialysis, the beads were stored in the wet state in 50 mL centrifuge tubes at ambient conditions. Control beads were prepared with 4% w/w CNC and 1% sodium alginate following the same procedure as above.

4.2.4 Batch Adsorption Experiments

To test the adsorptive properties of the prepared hydrogel beads, batch adsorption experiments were conducted on MO and KPFBS.

4.2.4.1 Adsorption of MO by TF-CNC and TF-CNC-ALG Beads

MO solutions of varying concentrations were prepared and the adsorbent (15 mg TFSG-CNC, 25 mg TFSH-CNC, or 30 mg dry weight of the beads) was added to each solution. The solutions were then allowed to equilibrate overnight on a shaker. The adsorbent was removed from the MO solution through filtration (beads) or ultracentrifugation at 15000 rpm for 10 minutes (TF-CNC). The UV-vis absorbance of the filtrates and supernatant solutions were measured at 464 nm using a Cary 100 Bio UV-vis spectrophotometer to determine the MO remaining in the solution.

4.2.4.2 Adsorption of KPFBS by TF-CNC-ALG Beads

40 mL of 250 µM KPFBS solution were prepared in 10 mM KCl. Hydrogel beads (300 mg dry weight) were added to the KPFBS solution. The solutions were allowed to equilibrate on a shaker (overnight for CNC-ALG and 4SG-ALG to allow equilibration; 3 hours for 4SH-ALG and 8SH-ALG to prevent bead disintegration). After adsorption, the solutions were centrifuged at 8500 rpm for 30 minutes. Ultrafiltration through a 0.1 µm membrane was used to remove any remaining particles from the supernatant. The KPFBS concentration in the filtrates was measured with a KPFBS ion-selective electrode (ISE).

4.3 Material Characterization

4.3.1 Quantification of Quaternary Ammonium Groups in TF

The amount of quaternary ammonium groups (QAG) in TF was determined via potentiometric titration with silver nitrate using a Metrohm Titrando system coupled with an Ag/AgCl reference electrode. TFSG and TFSH sample solutions (20 mL, 1 mg/mL) were titrated with 10 mM $AgNO_3$ solution, and the moles of quaternary ammonium groups per gram in each TF sample was calculated using the equation:

$$mol_{QAG} = \frac{V_T \times C_T}{m_{TF}} \qquad \text{(Eq. 12)}$$

where mol_{QAG} is the moles of QAG in the sample, V_T is the total volume of titrant added at the endpoint, C_T is the concentration of the titrant, and m_{TF} is the mass of TF in the sample in grams.

4.3.2 Hydrodynamic Size and Zeta Potential of TF-CNC

The hydrodynamic size and zeta potential (ZP) of the TF-CNC were determined using a Malvern Nano-ZS90 Zetasizer. Samples were prepared by diluting dispersed TF-CNC to 0.1% (w/w) in Milli-Q water. Samples were sonicated using a probe sonicator for 2 minutes before measurements were conducted. Hydrodynamic size measurements were conducted using single angle (90°) dynamic light scattering at room temperature, while ZP measurements were based on electrophoretic potential at room temperature. All measurements were repeated three times and data are presented as averages of the three measurements.

4.3.3 Fourier Transform Infrared Spectroscopy (FT-IR) of TF-CNC

FT-IR spectroscopy was conducted using a PerkinElmer 1720 FT-IR spectrometer to validate CNC modification. Samples were prepared by grinding them with KBr and using a hydraulic press to form transparent pellets. The pellets were scanned using the spectrometer at a resolution of 4 cm^{-1} to obtain the spectra.

4.3.4 Coating Efficiency of TF

To determine the amount of TF coated onto CNCs, TF-CNC were centrifuged after the coating process to remove excess TF. The supernatant was collected, and the concentration of TF was measured using a Cary 100 Bio UV-vis spectrophotometer at 285 nm and 284 nm for TFSH and TFSG, respectively. The amount of TF in the solution was determined using the calibration curves constructed for TFSG and TFSH. The ratio of TF:CNC in the coated product was determined using the equation:

$$Coated\ TF = \frac{TF_0 - TF_E}{m_{CNC}} \qquad\qquad\qquad (\text{Eq. 13})$$

where TF_0 is the mass of TF added to the CNC dispersion, TF_E is the amount of excess TF determined through UV-vis spectroscopy, and m_{CNC} is the mass of CNC in the dispersion.

4.3.5 Hydrogel Bead Moisture Content and Diameter

The moisture content of the TF-CNC-ALG beads was determined using a VWR-54M.I Moisture Analyzer. Beads were removed from water and gently patted dry on a piece of Whatman Grade 1 filter paper to remove excess water before measurement.

The diameter of the hydrogel beads was measured using a pair of calipers. Beads were removed from water and patted dry on filter paper. The diameters of 15 beads were measured and the data presented are averages of 15 measurements.

4.4 Results and Discussion

4.4.1 Quaternary Ammonium Content of TFSH and TFSG

The QAG in TFSH and TFSG were determined using silver nitrate titration. The volume of titrant (10 mM $AgNO_3$) required to neutralize the chloride counterions present in solution was determined using the titration curves (Figure 29), and Eq. 12 was used to calculate 0.20 mol_{QAG}/g for both TFSH and TFSG. These values have not been reported previously in the literature to the author's knowledge.
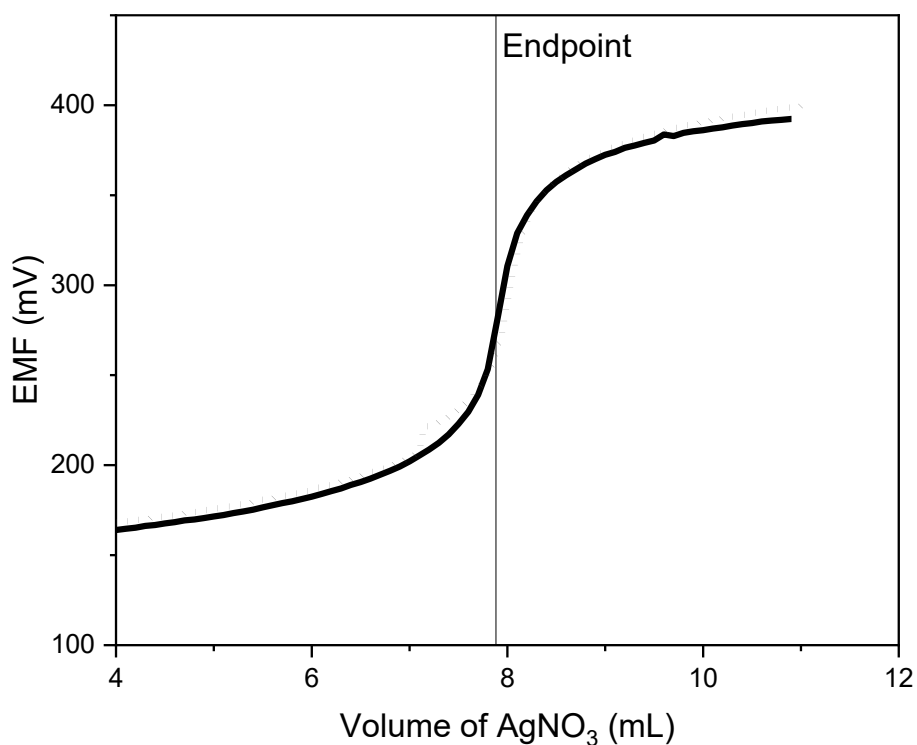
Figure 29: Silver nitrate titration curves for TF. The solid line represents TFSH and the dotted lined represents TFSG.

4.4.2 pH Response of TF

To determine the suitability of TF at different pH conditions, the zeta potential and size of TFSH and TFSG were determined over a pH range of 2-11. The pH of the TF solutions was controlled with 1 M and 0.1 M NaOH and HCl. Both TFSG and TFSH showed positive zeta potential values at acidic pH values (Figure 30a-b). The point of zero charge for TFSH was between pH 9 and 10, and at pH 8 for TFSG. Both types of TF showed large particle sizes at pH 8, which occurs due to particle aggregation at the point-of-zero-charge. The positive zeta potential at pH values below 8 makes TFSH and TFSG suitable for water treatment at neutral and acidic conditions.
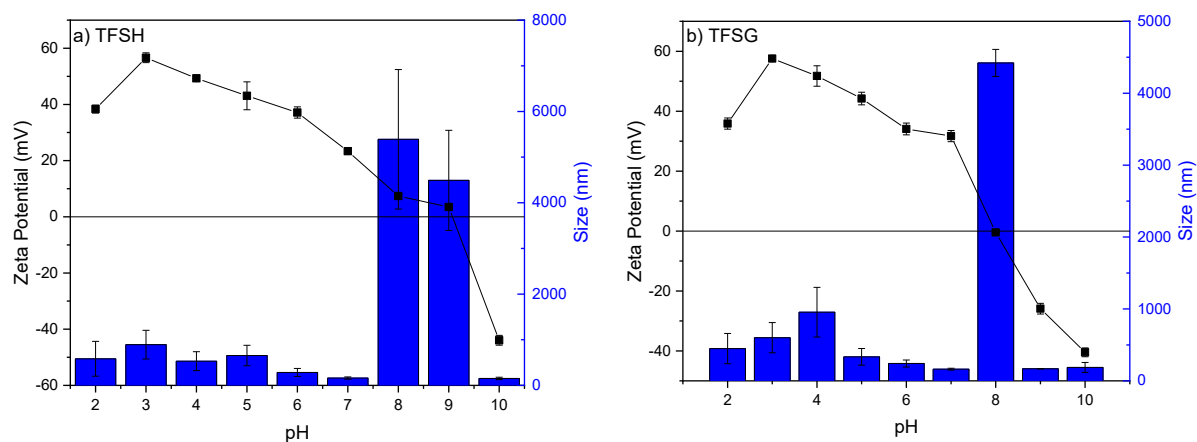
Figure 30: The dependence of the size and zeta potential of a) TFSH and b) TFSG on solution pH.

4.4.3 Optimization and Characterization of TF-CNC Preparation

To determine the ratio of TF to CNC that provides the best coating and size and zeta potential, TF:CNC mass ratios from 0.5:1 to 3:1 were studied. The amount of TF in excess was determined using the calibration curves (Figure 31a-b). From the UV-vis measurements, it was determined that the amount of TF coated onto CNCs increased with the increasing amount of

TF added to the CNC dispersion for both TFSH and TFSG (Figure 32a). TFSH was determined

to be more efficient at coating CNCs, resulting in higher coating amounts for all tested ratios

except 0.5:1. 1:1 coating was achieved with starting ratios of 1.5:1 and 2.5:1 for TFSH and

TFSG, respectively.
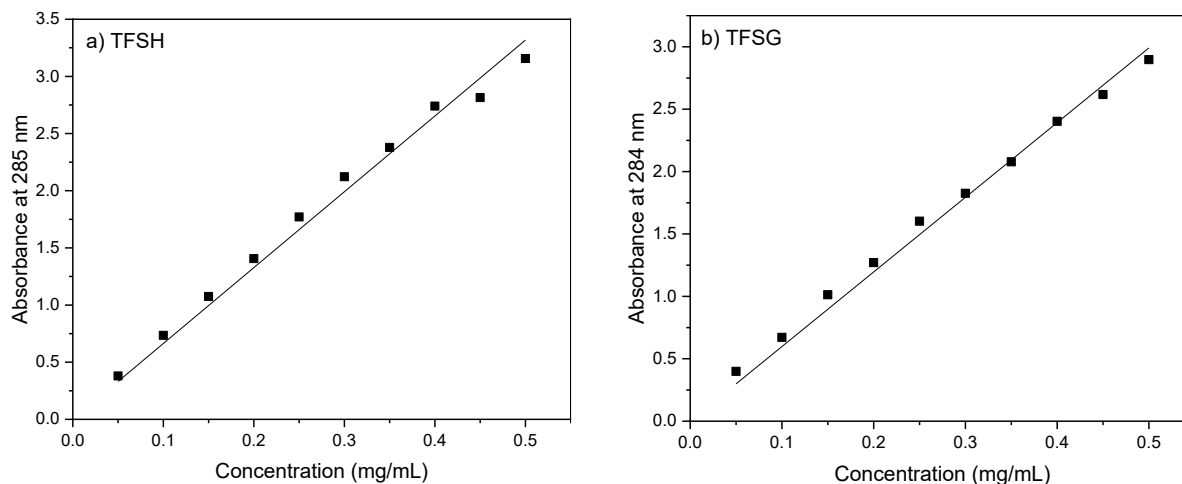
Figure 31: UV-vis calibration curves for a) TFSH (y = 6.63602x, R^2 = 0.99697) and b) TFSG (y = 5.98056x, R^2 = 0.99802).

A 2:1 TF:CNC starting ratio was determined to yield coated CNCs with the largest

positive zeta potential for both TFSH and TFSG (Figure 32b), with TFSG-CNCs having a more

positive surface charge of +44.2 ± 1.0 mV than TFSH-CNCs (+39.2 ± 7.0 mV). Since zeta

potential is expected to increase or remain constant with increasing TF:CNC ratios after

reaching a maximum value, the drop in zeta potential at TF:CNC 2.5:1 is likely due to

experimental error. The largest particle size was observed at an initial TF:CNC ratio of 0.5:1

for TFSH-CNCs and 1:1 for TFSG-CNCs. Due to the highly positive zeta potential, small

particle size, and good coating efficiency, the TF:CNC ratio of 2:1 was determined to be the

optimal ratio for the coating of CNCs with TF. All the experiments were conducted at the latent pH of the solutions (~6).

To determine the amount of time required to achieve maximum coating of CNCs by TF, six samples with TF:CNC ratios of 3:1 were prepared with a stirring time from 0 to 5 days. The initial ratio of 3:1 was selected to determine if there was a maximum coating that could be achieved. The stirring time was found to have no effect on the coating of TFSH onto CNCs (Figure 33a). However, a stirring time of 2 days resulted in the highest coating of TFSG onto CNCs (1.7:1), and the amount of coated TF decreased when the samples were allowed to stir for 3 to 5 days. Hydrodynamic size measurements showed no effect of stirring time on TFSG-CNC particle size between 0 and 4 days of stirring and showed a slight increase in the particle size from 228.7 ± 14.4 nm to 292.8 ± 13.0 nm after 5 days (Figure 33b). TFSH-CNC showed a large particle size and distribution (614.4 ± 322.1 nm) with a stirring time of 0 days. However, stirring for 1 to 5 days resulted in smaller particle sizes of approximately 230 nm, with smaller standard deviations. The most positive zeta potential values were obtained after 1 day of
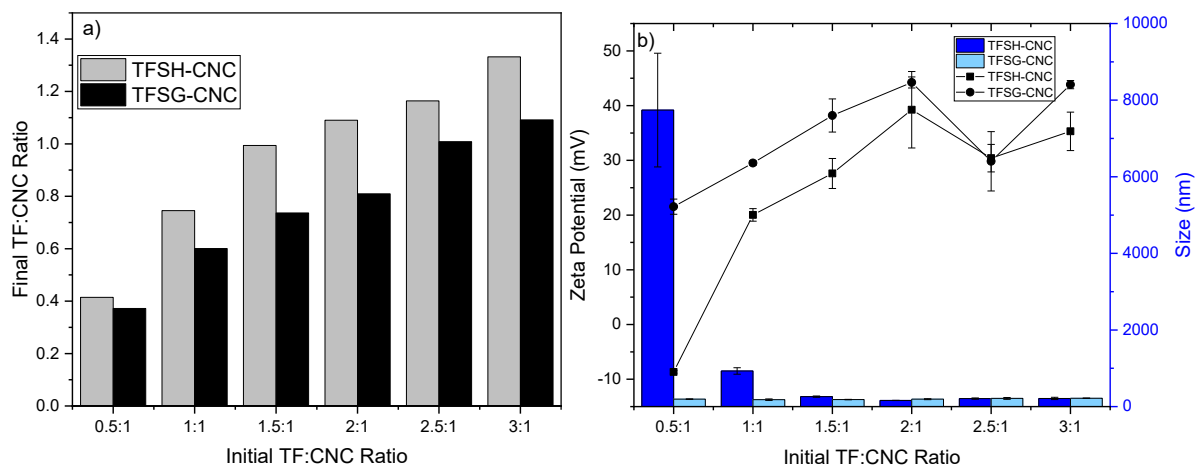
Figure 32: The dependence of a) coating amount and b) size and zeta potential on the initial TF:CNC ratio.
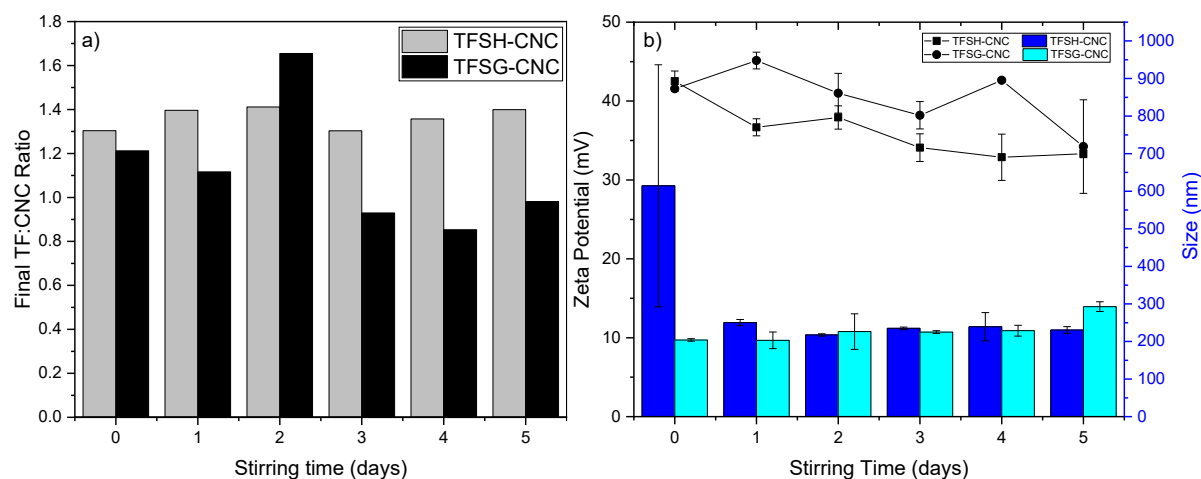
Figure 33: The effect of stirring time on a) TF coating efficiency and b) size and zeta potential.

stirring for TFSG-CNC (+45.1 ± 1.1 mV) and after 0 days of stirring for TFSH-CNC (+42.5 ± 1.3 mV). However, due to the large particle size distribution at 0 days of stirring, the optimal time for TFSH-CNC preparation was determined to be 2 days. The optimal time for the preparation of TFSG-CNC was also determined to be 2 days, due to the high coating efficiency, positive zeta potential, and consistent particle size.

The parameters determined in this section were used to prepare adsorbents containing TFSH-CNC and TFSG-CNC by incorporating them into hydrogel beads. A summary of these parameters is given in Table 2.

Table 2: Optimal Ratio and Stirring Time for TF-CNC Preparation

Parameter	TFSH-CNC	TFSG-CNC
TF:CNC Ratio	2:1	2:1
Stirring Time (days)	2	2

FT-IR spectroscopy was conducted to validate the coating of CNCs with TF. The spectra of both TFSH-CNC and TFSG-CNC (Figure 34a-b) showed decreasing peak intensities of the cellulose C-H sp^2 stretching bands at 2900 cm^{-1} with increasing TF:CNC ratios, while the characteristic cellulose peaks in the 950 cm^{-1} to 1163 cm^{-1} region increased in intensity in

the coated samples. The coated samples also showed an increase in the C-H bending bands at 1430 and 1470 cm^{-1} that are present in TFSH and TFSG. The differences in peak intensities were slight because the amount of TF coated onto the CNCs was not drastically different
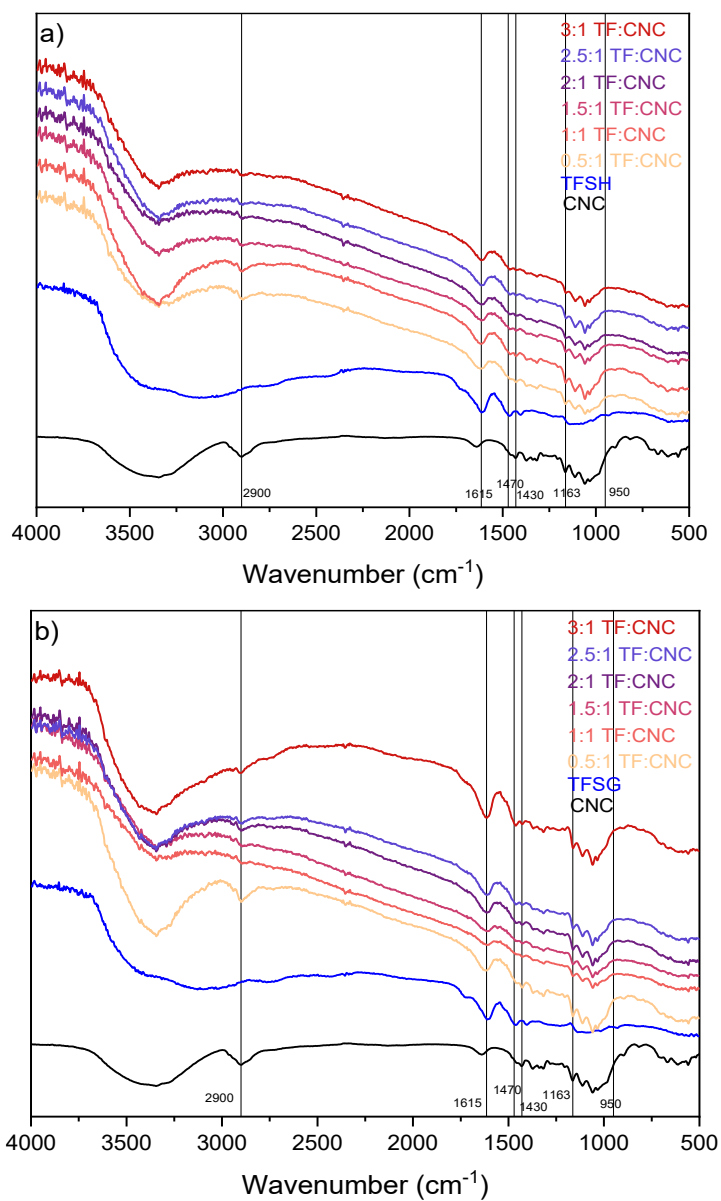
Figure 34: FT-IR spectra of a) TFSH-CNC and b) TFSG-CNC with varying ratios of TF:CNC.

between samples. Finally, the coated samples showed the appearance of intense N-H bending bands at 1615 cm^{-1}, confirming the successful coating of both TFSH and TFSG onto CNCs.

4.4.4 Adsorptive Properties of Hydrogel Beads and Coated CNCs

Four batches of hydrogel beads were prepared to study the absorptive properties of the TF-CNC material: CNC-ALG control beads, hydrogel beads containing 4% TFSH-CNC (4SH-ALG), hydrogel beads containing 8% TFSH-CNC (8SH-ALG), and hydrogel beads containing 4% TFSG-CNC (4SG-ALG). The CNC-ALG beads and 4SG-ALG beads showed consistent, spherical shapes and sizes, while the 4SH-ALG and 8SH-ALG beads were more elongated in shape and less robust (Figure 35). All hydrogel beads containing coated CNCs were brown in colour, corresponding to the colour of Tanfloc in solution. 4SH-ALG beads showed a less intense brown colour than 8SH-ALG beads, an indication of lower TFSH content in the beads. The moisture content and diameters of the beads were measured and are reported in Table 3.
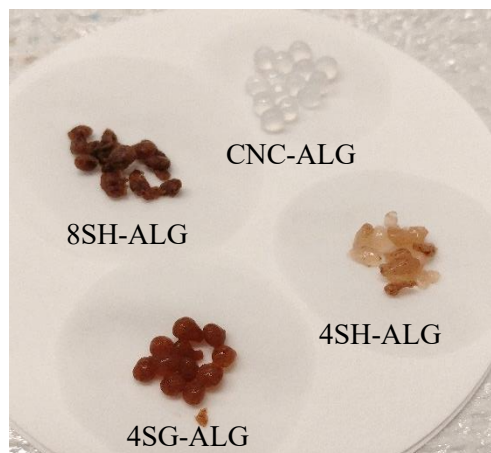
Figure 35: Photograph of different hydrogel beads prepared.

Table 3: Composition, diameter, and moisture content of hydrogel beads.

System Name	(TF)-CNC Content	Alginate Content	Diameter (mm)	Moisture Content (%)
CNC-ALG	2% CNC	0.5%	3.10 ± 0.06	92.6
4SH-ALG	2% TFSH-CNC	0.5%	3.02 ± 0.21	94.8
4SG-ALG	2% TFSG-CNC	0.5%	3.00 ± 0.03	90.1
8SH-ALG	4% TFSH-CNC	0.5%	2.98 ± 0.25	86.6

Batch adsorption experiments were conducted to study the adsorptive properties of the prepared hydrogel beads for MO chosen as a model compound due to its anionic nature. Solutions with varying concentrations of MO were treated with the hydrogel beads. To confirm that an increase in adsorption of the TF-CNC-ALG beads was due to the TF coating on the CNCs, CNC-ALG beads prepared with pristine CNCs were tested. Fitting the plot of q_e against C_e (Figure 36) to the Langmuir isotherm yielded a q_{max} of 2.2 mg/g and a K_L of 0.0022 L/mg.
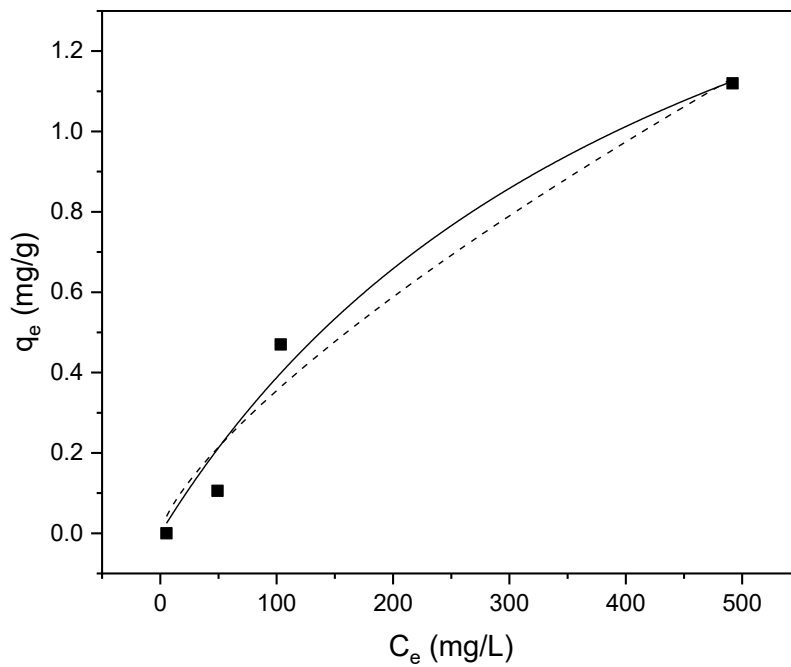
Figure 36: Isotherm plots of the adsorption of MO by CNC-ALG hydrogel beads. The filled squares represent experimental data, the solid line represents Langmuir isotherm fitting, and the dashed line represents Freundlich isotherm fitting.

The Langmuir isotherm showed better fitting to the data than the Freundlich isotherm, with R^2 values of 0.97 and 0.95, respectively.

Batch adsorption experiments with 4SG-ALG showed a slightly larger q_{max} of 3.8 mg/g compared to the CNC-ALG beads, with a K_L of 0.0011 L/mg, with an R^2 of 0.93, making the Langmuir isotherm a better fit than the Freundlich isotherm (Figure 37a), which had an R^2 of
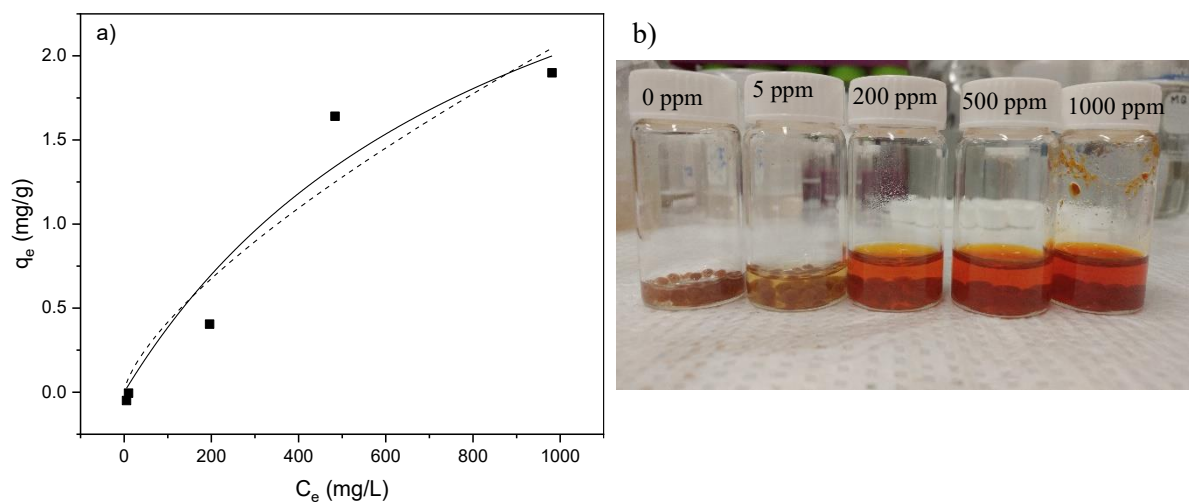
Figure 37: a) Isotherm plots of the adsorption of MO with 4SG-ALG hydrogel beads. The solid squares represent experimental data, the solid line represents Langmuir isotherm fitting, and the dashed line represents Freundlich isotherm fitting. b) Photograph of 4SG-ALG beads in sample solutions after the batch adsorption tests.

0.90. The beads remained intact in the sample solutions after the batch adsorption experiments (Figure 37b), showing that they are robust.

Batch adsorption of MO with 4SH-ALG yielded an increasing q_e with increasing initial dye concentration (Figure 38a). The removal efficiency also increased slightly above initial MO concentrations of 500 ppm, although the maximum removal achieved was only 22.5% (Figure 38b). The hydrogel beads were observed to have disintegrated during the adsorption test, indicating that the calcium ion crosslinking between the TFSH-CNC and the ALG was weak.

Batch adsorption with 8SH-ALG showed a similar trend to that observed for 4SH-ALG, with increasing dye adsorption with increasing initial MO concentration (Figure 38c). However, the removal percentage for 8SH-ALG was significantly higher than 4SH-ALG, with the adsorbent showing 95% removal for the initial MO concentration of 5 ppm and 99.7% removal for 200 ppm (Figure 38d). The 8SH-ALG beads also disintegrated during the batch tests (Figure 39a), indicating weak crosslinking with calcium ions.
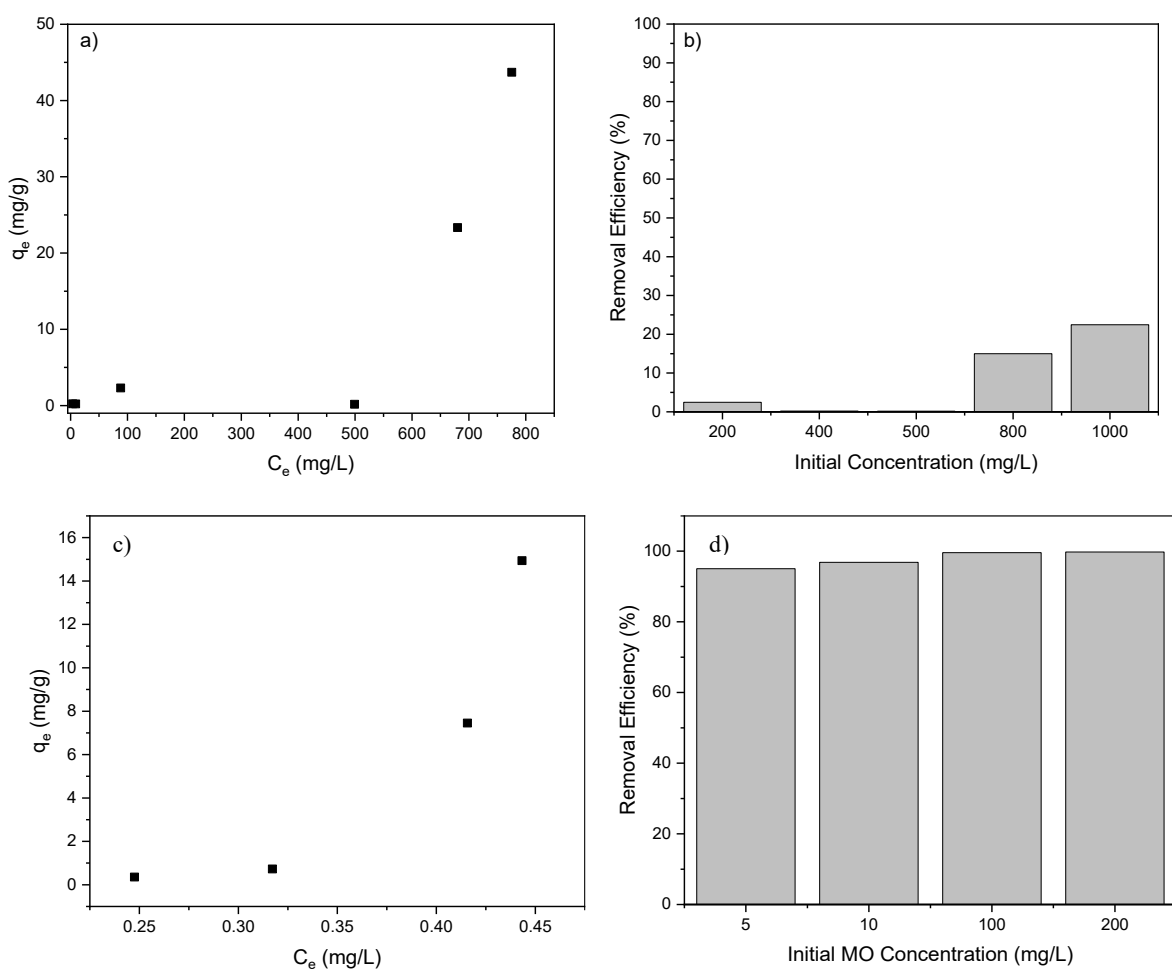
Figure 38: a) Plot of adsorbed dye vs equilibrium MO concentration for 4SH-ALG as the adsorbent, b) the removal efficiency of MO by 4SH-ALG, c) plot of adsorbed dye vs equilibrium MO concentration for 8SH-ALG as the adsorbent, and d) the removal efficiency of MO by 8SH-ALG.

To prevent the disintegration of the beads, the adsorption experiment was repeated with an adsorption time of 2 hours rather than equilibrating overnight. To ensure that 2 hours was sufficient for the system to reach equilibrium, a 100 ppm MO solution was contacted with 8SH-ALG for 180 minutes and the resulting MO concentration remaining in solution was monitored (Figure 39b). This experiment showed that equilibrium was reached within 60 minutes.
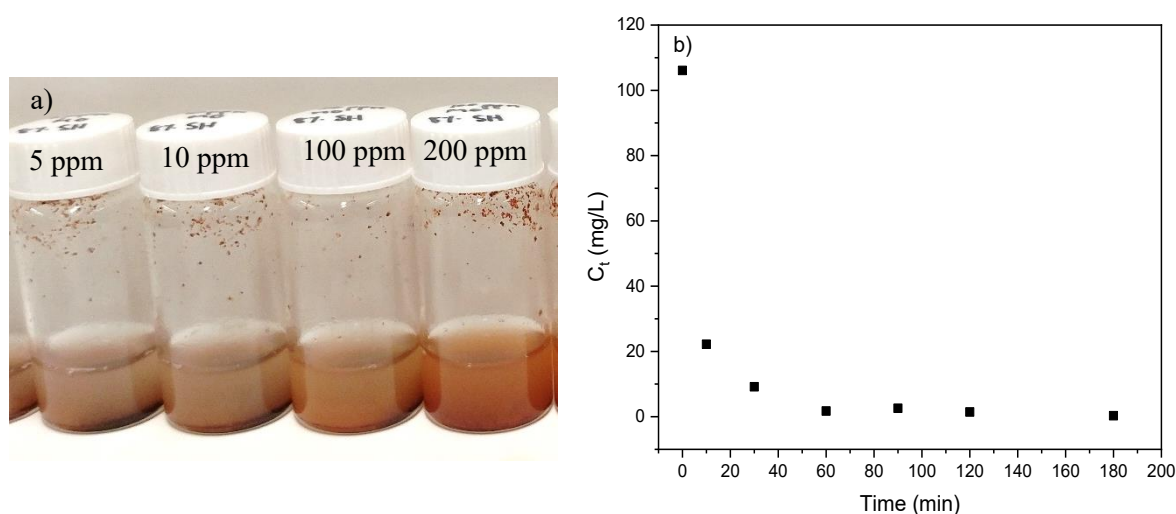
Figure 39: a) Disintegrated 8SH-ALG beads after batch tests with MO and b) determination of time required to reach equilibrium in MO adsorption tests with 8SH-ALG (initial MO concentration: 100 ppm).

MO adsorption with 8SH-ALG for 2 hours resulted in the beads remaining intact relative to the previous experiment (Figure 40a). Fitting the Langmuir and Freundlich isotherms to the experimental data (Figure 40b) resulted in R^2 values of 0.93 and 0.98 for the two isotherms, respectively. The predicted K_F and n values for the adsorbent were 1.02 $(mg/g)(L/mg)^{1/n}$ and 4.2, respectively, while Langmuir isotherm fitting predicted a q_{max} value of 4.9 mg/g.
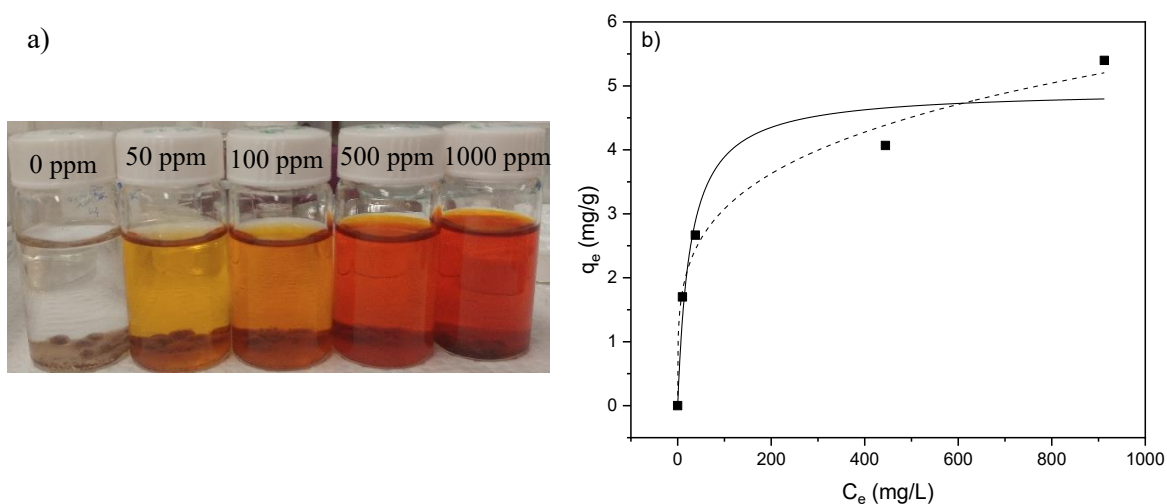
**Figure 40: a) Photograph of 8SH-ALG beads in MO after adsorption for 2 hours and b) isotherm plots of the adsorption of MO with 8SH-ALG hydrogel beads. The solid squares represent experimental data, the solid line represents the fitted Langmuir isotherm, and the dashed line represents the fitted Freundlich isotherm.**

The results reported above showed significantly different removal efficiencies, adsorptive behaviour, and appearance of the hydrogel bead systems. The CNC-ALG beads were robust, with well-defined shapes, as reported previously [71]. While the 4SH-ALG beads showed similar consistency in appearance, the 4SH-ALG and 8SH-ALG beads were less spherical and robust. The 4SH-ALG beads were light brown in colour and soft in texture, while the 8SH-ALG beads were darker and relatively more robust. The difference in robustness was due to the differing CNC content of the beads. Since TFSG has a lower coating efficiency than TFSH (Figure 32a), the final CNC content of the 4SG-ALG beads was higher than that of the 4SH-ALG beads, leading to the formation of more robust beads. The 8SH-ALG beads were more robust than 4SH-ALG beads because they contained a higher final CNC content.

From the batch adsorption tests, the low q_{max} of the control CNC-ALG beads indicated that pristine CNCs do not show significant uptake of MO. This result was expected due to electrostatic repulsion between the anionic MO molecules and the negatively charged CNCs, confirming that unmodified CNCs do not efficiently remove anionic species from water. The predicted q_{max} values for the TF-CLC-ALG systems were only slightly larger than the CNC-ALG hydrogel beads. It is possible that due to the positive surface charge of the TF-CNC, the TF-CNC acted as the crosslinker during hydrogel bead formation rather than the calcium ions [84]. This would result in fewer positively charged sites on the adsorbent for the anionic species in water to interact with and reduce the adsorption capacity of the adsorbent.

The adsorption and removal of MO by 4SH-ALG and 8SH-ALG beads was much greater when the beads disintegrated in the sample solutions (Figure 38). The disintegration of the beads resulted in the release of positively charged TF-CNC into the solution, as well as any calcium ions that were involved in the crosslinking, while also increasing the surface area for interactions with MO molecules. The positively charged particles were then able to interact with the anionic MO molecules present in the solution and remove the anions from solution. The increase in the ionic strength of the solution could also have contributed to the salting out of MO from solution [102], increasing the apparent q_e values. Another possible cause for the increase in removal efficiency is the interaction of MO molecules with each other, resulting in stacking and greater removal at higher initial MO concentrations [103]. These data suggest that the use of sodium alginate as the hydrogel network is not suitable for the removal of anionic species from water.

70

Data from 8SH-ALG as the adsorbent showed better fitting to the Freundlich isotherm (a summary of the fitting parameters is provided in Table 4), which may be due to the heterogeneity in the amount of TFSH-CNC incorporated into the beads, resulting in highly irregular distribution of the coated CNCs.

The overall performance of the hydrogel bead systems in the removal of MO from solution suggests that the beads are not suitable for the removal of anionic species from water. Based on the data obtained for MO, the beads were not expected to achieve high removal efficiencies for PFASs in water.

To confirm that the low adsorption capacity of the hydrogel beads was due to the encapsulation of the coated CNCs into the alginate network, the adsorption of MO onto TFSH-CNC and TFSG-CNC was tested. Both TFSH-CNC and TFSG-CNC showed significantly higher adsorption capacity than the hydrogel bead systems, with the predicted q_{max} values of 917.8 mg/g and 474.2 mg/g, respectively (Figure 41). The R^2 values for the fit were higher for
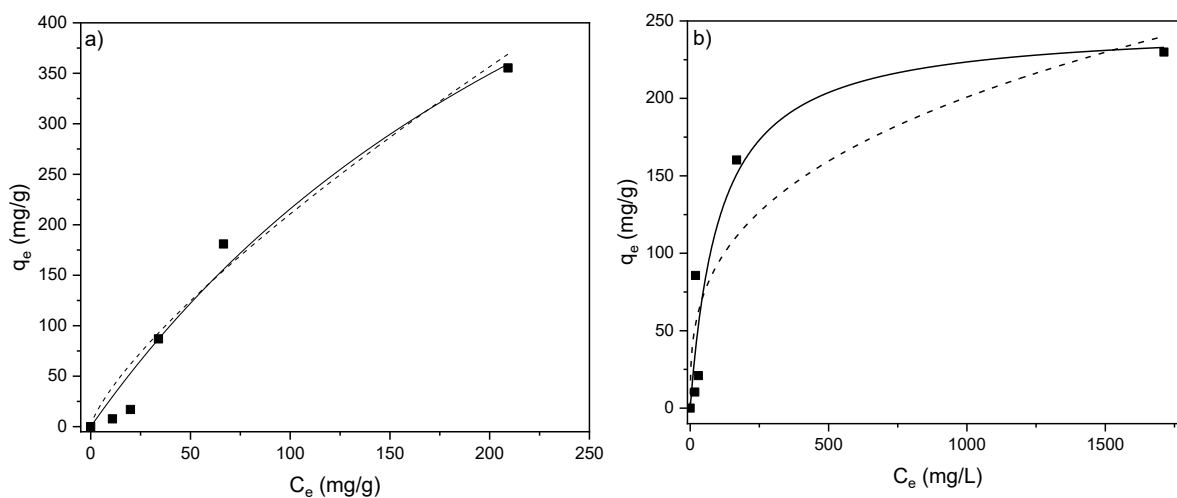
Figure 41: Isotherm plots for the adsorption of MO onto a) TFSH-CNC and b) TFSG-CNC. Squares represent experimental data, solid lines represent Langmuir isotherm fitting, and dashed lines represent Freundlich isotherm fitting.

the Langmuir isotherm than the Freundlich isotherm for TFSG-CNC, indicating that the adsorption of MO by TFSG-CNC is better described by the Langmuir isotherm. However, both isotherms describe the adsorption of MO onto TFSH-CNC, as indicated by the similar R^2 values. The high q_{max} values of the coated CNCs suggest that TF-CNC is a promising adsorbent for the removal of anionic species from water. However, the reduction in adsorption capacity due to the encapsulation of TF-CNC into an alginate network suggests that alternate methods to incorporate TF-CNC into a practical adsorbent system are necessary.

Another limitation of the adsorption data presented here is the extrapolation of the models to obtain fitting parameters. The experiments were limited by the solubility of MO, and additional data should be collected by reducing the adsorbent mass added to dye solution to achieve saturation.

Table 4: Isotherm fitting parameters for hydrogel bead systems and coated CNCs.

System	Langmuir Isotherm			Freundlich Isotherm		
	q_{max} (mg/g)	K_L (L/mg)	R^2	K_F $(mg/g)(L/mg)^{1/n}$	n	R^2
CNC-ALG	2.2	0.0022	0.97	0.012	1.4	0.95
4SG-ALG	3.8	0.0011	0.93	0.017	1.4	0.90
8SH-ALG	4.9	0.037	0.93	1.02	4.2	0.98
TFSG-CNC	247.5	0.00931	0.89	20.2	3.0	0.80
TFSH-CNC	917.8	0.0031	0.97	6.38	1.3	0.99

Finally, the hydrogel bead systems were used to treat 250 µM KPFBS. All bead systems containing TF-CNC achieved higher removal of KPFBS than the CNC-ALG control (Figure

42). This indicates that the coating of CNC with positively charged TF improved the adsorption capacity of CNCs for negatively charged targets such as PFAS. The highest removal (38.2%) was achieved by 8SH-ALG hydrogel beads, with 4SH-ALG and 4SG-ALG beads achieving 26.1% and 34.9% removal, respectively. The higher removal by 8SH-ALG beads was due to the higher content of coated CNCs in the beads, resulting in more adsorption sites available for the KPFBS. The modest removal efficiencies of the hydrogel bead systems indicate the need
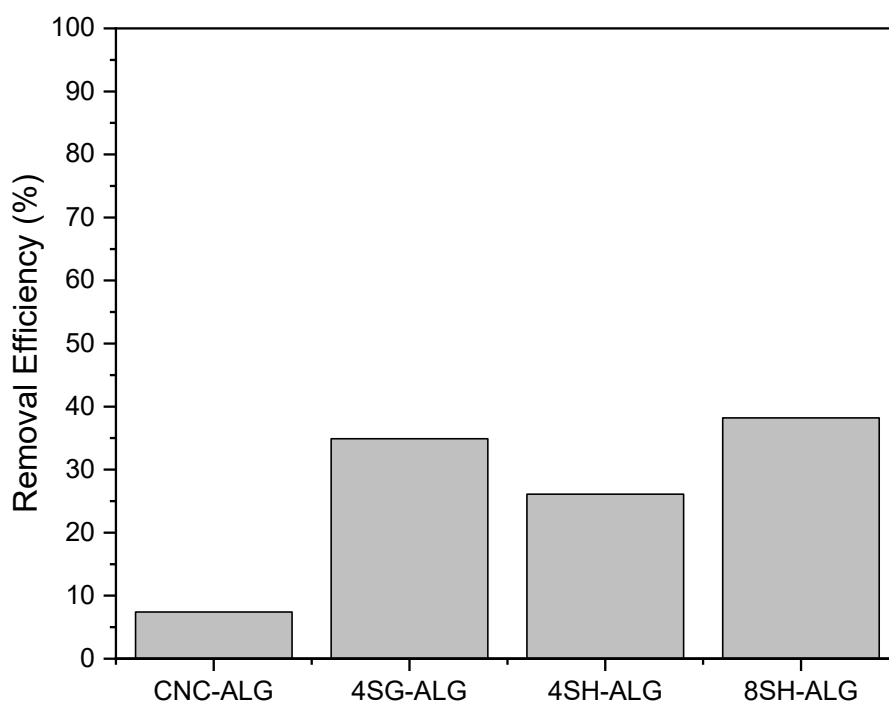
Figure 42: KPFBS removal by different hydrogel bead systems. Initial concentration of KPFBS = 250 μM.

for further optimization of the system. Limiting the treatment time to 2 hours prevented the disintegration of the beads. This indicates that the beads can achieve removal of KPFBS while maintaining their structural integrity.

4.5 Conclusions

This chapter presents the coating of CNCs with a commercial, lignin-based flocculant, Tanfloc, and the incorporation of the coated CNCs into a hydrogel bead network consisting of sodium alginate.

Starting ratios of 2:1 TF:CNC and stirring times of 2 days were determined to be optimal for the coating of TFSH and TFSG onto CNC, and produced TF-CNCs with highly positive zeta potential values (+35-40 mV). Hydrogel beads incorporating TF-CNC into an ALG network were prepared and used as adsorbents to test the removal of the anionic dye MO. Batch adsorption tests showed low q_{max} values for the TF-CNC-ALG bead systems, but removal efficiencies of up to 99% were achieved when the beads disintegrated in the solution. These results indicate that ALG hydrogel beads with TF-CNC are not suitable for highly efficient removal of anionic species from water. However, the increase in removal efficiency with increased surface area and the release of TF-CNC particles in solution, as well as the high q_{max} values for TFSH-CNC and TFSG-CNC indicated that the system holds promise as an adsorbent, and optimal parameters and conditions to exploit these adsorptive properties should be studied in detail.

The treatment of KPFBS with the produced hydrogel bead systems resulted in removal efficiencies between 26.1 and 38.2%, with the highest removal efficiency achieved by 8SH-ALG beads. Despite the low removal efficiencies, all hydrogel beads containing TF-CNC achieved higher KPFBS removal than pure CNC-ALG control beads, suggesting that the coated CNCs are a promising adsorbent system for PFAS remediation. Further studies on the

development of robust systems incorporating coated CNCs should be conducted to study the

maximum PFAS remediation potential of TF-CNC.

Chapter 5: Conclusions and Recommendations for Future Work

5.1 Conclusions

The goal of this study is to prepare sustainable adsorbents for the removal of PFASs from water, and this was achieved through physical and chemical modification of cellulose nanocrystals.

CNCs were chemically modified with GTMAC to produce cationic CNCs and with β-CD to produce β-CD-grafted CNCs. GCNC was produced to remove PFASs from water through electrostatic interactions while β-CD-CNC was used to exploit the host-guest interactions that β-CD is known to make with PFASs such as PFOA.

Cellulose nanocrystals were coated with two forms of the cationic, lignin-based flocculant, Tanfloc, to produce positively charged TF-CNC. The simple coating procedure was optimized to produce coated CNCs with highly positive (+35-40 mV) surface charge using starting TF:CNC mass ratios of 2:1 and allowing the coating to occur over 2 days. The coated CNCs were then used to prepare hydrogel beads through ionotropic gelation with sodium alginate and tested as adsorbents for the uptake of anionic species.

Methyl orange was used as a model compound to test the adsorptive properties of the adsorbents. Batch adsorption tests showed increasing MO removal with increasing initial MO concentration for GCNC, with the highest removal efficiency of 80% at 1000 ppm MO, suggesting that the GCNC may be suitable for the removal of anionic species from water at high concentrations. Conversely, the dye removal efficiency for β-CD-CNC was highest at an initial MO concentration of 20 ppm (71% removal), and the maximum adsorption capacity obtained from fitting the data to the Langmuir isotherm was 125.7 mg/g. This suggests that β-CD-CNC is suitable for the removal of anionic species at low initial concentrations.

All the hydrogel bead systems had low adsorption capacities, although there was a 73% increase in q_{max} when 4% TFSG-CNC was used to prepare the beads, and a 122% increase in q_{max} when 8% TFSH-CNC was used. When the beads disintegrated in the MO solutions and released the coated CNC particles, the increase in the number of sites for electrostatic interactions improved MO removal, and up to 99.7% removal was achieved at 200 ppm MO with the 8SH-ALG hydrogel beads. Further, when TFSH-CNC and TFSG-CNC were tested without impregnation into an alginate matrix, the respective q_{max} values of 917.8 mg/g and 247.5 mg/g were found.

All adsorbents were used to remove KPFBS from water to test their performance against PFAS. GCNC and β-CD-CNC achieved removal efficiencies of 43.7 and 56.5%, respectively, showing promise for the removal of short-chain PFAS from water. The treatment of KPFBS with the hydrogel bead systems resulted in removal efficiencies ranging from 26.1 to 34.9%, indicating that TF coatings improve the PFAS adsorption capacity of CNCs, and TF-CNCs are promising for the removal of short chain PFAS from water. The chemically modified CNCs showed better removal efficiencies for KPFBS compared to the hydrogel beads. These results indicate that while Tanfloc-coated CNCs do improve the adsorption of anionic species by CNCs, sodium alginate is not a desirable hydrogel matrix for the incorporation of TF-CNC.

5.2 Recommendations for Future Work

Future work on this project should focus on improving the grafting efficiencies of GTMAC and β-CD onto CNC. Improved GTMAC grafting could be achieved by using organic solvents to prevent hydrolysis of GTMAC. A dry method without the use of solvents should also be investigated for a more environmentally friendly reaction procedure. To improve the

grafting of β-CD onto CNC, different crosslinkers such as decafluorobiphenyl could be used rather than epichlorohydrin [70]. Additionally, the ratio of β-CD to crosslinker could be optimized to improve the grafting efficiency. The synthesis of CNCs which are both cationic and grafted with β-CD should also be considered to simultaneously utilize both electrostatic and hydrophobic host-guest interactions during water treatment.

Since sodium alginate is not a desirable hydrogel network for the incorporation of coated CNCs due to its negative charge, a positively charged system should be investigated instead. Once such system is the well-established chitosan-tripolyphosphate hydrogel bead system [104]. Because chitosan is positively charged, the incorporation of TF-CNCs into chitosan-based beads is expected to enhance the adsorption capacity of the adsorbent for anionic species such as MO and PFAS. The longevity of the TF coating on CNC should also be studied in detail, as changes in the coating may have a significant effect on the adsorptive properties of the material.

To better understand the adsorption mechanisms involved in the uptake of PFASs from water by these adsorbents, the dynamics of adsorption should be studied in detail. This will allow a thorough understanding of intraparticle mass transfer and reaction kinetics, factors which are important for process design. The effect of factors such as salt content, presence of competitive ions, solution pH, solution temperature, and dissolved organic matter should also be studied. These studies will provide a thorough understanding of the affinity and specificity of the adsorbents for PFASs present in water samples. Adsorption tests with real environmental samples containing competitive species should also be conducted to determine the applicability of the adsorbents to water treatment plants.

Finally, the disposal of the collected PFASs should also be seriously considered. Current studies reported in the literature primarily focus on the removal of PFASs from water and do not discuss the fate of the removed PFASs. It is vital to ensure that the disposal of spent adsorbents does not reintroduce PFASs into the environment. Therefore, methods that convert PFASs to benign species or destroy them completely should be developed.

References

[1] S. Rayne and K. Forest, "Perfluoroalkyl sulfonic and carboxylic acids: A critical review of physicochemical properties, levels and patterns in waters and wastewaters, and treatment methods," *J. Environ. Sci. Heal. Part A*, vol. 44, no. 12, pp. 1145–1199, Sep. 2009, doi: 10.1080/10934520903139811.

[2] K. Shinoda, M. Hatö, and T. Hayashi, "The physicochemical properties of aqueous solutions of fluorinated surfactants," *J. Phys. Chem.*, vol. 76, no. 6, pp. 909–914, 1972, doi: 10.1021/j100650a021.

[3] R. C. Buck *et al.*, "Perfluoroalkyl and polyfluoroalkyl substances in the environment: Terminology, classification, and origins," *Integr. Environ. Assess. Manag.*, vol. 7, no. 4, pp. 513–541, Oct. 2011, doi: 10.1002/ieam.258.

[4] V. M. Vieira, K. Hoffman, H. M. Shin, J. M. Weinberg, T. F. Webster, and T. Fletcher, "Perfluorooctanoic acid exposure and cancer outcomes in a contaminated community: A geographic analysis," *Environ. Health Perspect.*, vol. 121, no. 3, pp. 318–323, 2013, doi: 10.1289/ehp.1205829.

[5] T. C. Su, C. C. Kuo, J. J. Hwang, G. W. Lien, M. F. Chen, and P. C. Chen, "Serum perfluorinated chemicals, glucose homeostasis and the risk of diabetes in working-aged Taiwanese adults," *Environ. Int.*, vol. 88, pp. 15–22, Mar. 2016, doi: 10.1016/j.envint.2015.11.016.

[6] J. L. A. Pennings *et al.*, "Cord blood gene expression supports that prenatal exposure to perfluoroalkyl substances causes depressed immune functionality in early childhood," *J. Immunotoxicol.*, vol. 13, no. 2, pp. 173–180, Mar. 2016, doi: 10.3109/1547691X.2015.1029147.

[7] M. F. Rahman, S. Peldszus, and W. B. Anderson, "Behaviour and fate of perfluoroalkyl and polyfluoroalkyl substances (PFASs) in drinking water treatment: A review," *Water Res.*, vol. 50, pp. 318–340, 2014, doi: 10.1016/j.watres.2013.10.045.

[8] T. Stoiber, S. Evans, A. M. Temkin, D. Q. Andrews, and O. V Naidenko, "PFAS in drinking water: an emergent water quality threat," *Water Solut.*, pp. 40–49, 2020, Accessed: Mar. 28, 2021. [Online]. Available: www.ewg.org/interactive-maps/2019_pfas_contamina-.

[9] F. Rodríguez-Reinoso and M. Molina-Sabio, "Activated carbons from lignocellulosic materials by chemical and/or physical activation: an overview," *Carbon N. Y.*, vol. 30, no. 7, pp. 1111–1118, 1992, doi: 10.1016/0008-6223(92)90143-K.

[10] R. H. Hailemariam, Y. C. Woo, M. M. Damtie, B. C. Kim, K. D. Park, and J. S. Choi, "Reverse osmosis membrane fabrication and modification technologies and future trends: A review," *Adv. Colloid Interface Sci.*, vol. 276, p. 102100, Feb. 2020, doi: 10.1016/j.cis.2019.102100.

[11] M. J. Weiss-Errico and K. E. O'Shea, "Detailed NMR investigation of cyclodextrin-perfluorinated surfactant interactions in aqueous media," *J. Hazard. Mater.*, vol. 329, pp. 57–65, 2017, doi: 10.1016/j.jhazmat.2017.01.017.

[12] A. Su and K. Rajan, "A database framework for rapid screening of structure-function relationships in PFAS chemistry," *Sci. Data*, vol. 8, no. 1, pp. 1–10, Dec. 2021, doi:

10.1038/s41597-021-00798-x.

[13]   M. F. Rahman, S. Peldszus, and W. B. Anderson, "Behaviour and fate of perfluoroalkyl and polyfluoroalkyl substances (PFASs) in drinking water treatment: A review," *Water Res.*, vol. 50, pp. 318–340, Mar. 2014, doi: 10.1016/j.watres.2013.10.045.

[14]   E. Gagliano, M. Sgroi, P. P. Falciglia, F. G. A. Vagliasindi, and P. Roccaro, "Removal of poly- and perfluoroalkyl substances (PFAS) from water by adsorption: Role of PFAS chain length, effect of organic matter and challenges in adsorbent regeneration," *Water Res.*, vol. 171, p. 115381, Mar. 2020, doi: 10.1016/j.watres.2019.115381.

[15]   J. J. MacInnis, I. Lehnherr, D. C. G. Muir, R. Quinlan, and A. O. De Silva, "Characterization of perfluoroalkyl substances in sediment cores from High and Low Arctic lakes in Canada," *Sci. Total Environ.*, vol. 666, pp. 414–422, May 2019, doi: 10.1016/j.scitotenv.2019.02.210.

[16]   H. Joerss, C. Apel, and R. Ebinghaus, "Emerging per- and polyfluoroalkyl substances (PFASs) in surface water and sediment of the North and Baltic Seas," *Sci. Total Environ.*, vol. 686, pp. 360–369, 2019, doi: 10.1016/j.scitotenv.2019.05.363.

[17]   U. Eriksson and A. Kärrman, "World-Wide Indoor Exposure to Polyfluoroalkyl Phosphate Esters (PAPs) and other PFASs in Household Dust," *Environ. Sci. Technol.*, vol. 49, no. 24, pp. 14503–14511, 2015, doi: 10.1021/acs.est.5b00679.

[18]   G. Zheng, B. E. Boor, E. Schreder, and A. Salamova, "Indoor exposure to per- and polyfluoroalkyl substances (PFAS) in the childcare environment," *Environ. Pollut.*, vol. 258, p. 113714, Mar. 2020, doi: 10.1016/j.envpol.2019.113714.

[19]   A. Zhang *et al.*, "Occurrence and health risk of perfluoroalkyl acids (PFAAs) in seafood from Yellow Sea, China," *Sci. Total Environ.*, vol. 665, pp. 1026–1034, 2019, doi: 10.1016/j.scitotenv.2019.02.165.

[20]   R. Ghisi, T. Vamerali, and S. Manzetti, "Accumulation of perfluorinated alkyl substances (PFAS) in agricultural plants: A review," *Environ. Res.*, vol. 169, no. June 2018, pp. 326–341, 2019, doi: 10.1016/j.envres.2018.10.023.

[21]   B. M. Braune and R. J. Letcher, "Perfluorinated sulfonate and carboxylate compounds in eggs of seabirds breeding in the Canadian Arctic: Temporal trends (1975-2011) and interspecies comparison," *Environ. Sci. Technol.*, vol. 47, no. 1, pp. 616–624, 2013, doi: 10.1021/es303733d.

[22]   H. A. Kaboré *et al.*, "Worldwide drinking water occurrence and levels of newly-identified perfluoroalkyl and polyfluoroalkyl substances," *Sci. Total Environ.*, vol. 616–617, pp. 1089–1100, 2018, doi: 10.1016/j.scitotenv.2017.10.210.

[23]   T. A. Morck, F. Nielsen, J. K. S. Nielsen, V. D. Siersma, P. Grandjean, and L. E. Knudsen, "PFAS concentrations in plasma samples from Danish school children and their mothers," *Chemosphere*, vol. 129, pp. 203–209, Jun. 2015, doi: 10.1016/j.chemosphere.2014.07.018.

[24]   F. Pérez *et al.*, "Accumulation of perfluoroalkyl substances in human tissues," *Environ. Int.*, vol. 59, pp. 354–362, Sep. 2013, doi: 10.1016/j.envint.2013.06.004.

[25]   T. Zhang, H. Sun, X. Qin, Z. Gan, and K. Kannan, "PFOS and PFOA in paired urine and blood from general adults and pregnant women: assessment of urinary elimination," *Environ. Sci. Pollut. Res.*, vol. 22, no. 7, pp. 5572–5579, Apr. 2015, doi:

10.1007/s11356-014-3725-7.

[26] G. Zheng *et al.*, "Per- and Polyfluoroalkyl Substances (PFAS) in Breast Milk: Concerning Trends for Current-Use PFAS," *Environ. Sci. Technol.*, vol. 55, 2021, doi: 10.1021/acs.est.0c06978.

[27] S. Shah-Kulkarni *et al.*, "Prenatal exposure to perfluorinated compounds affects thyroid hormone levels in newborn girls," *Environ. Int.*, vol. 94, pp. 607–613, Sep. 2016, doi: 10.1016/j.envint.2016.06.024.

[28] M. Nian *et al.*, "Association between Prenatal Exposure to PFAS and Fetal Sex Hormones: Are the Short-Chain PFAS Safer?," *Environ. Sci. Technol.*, vol. 54, no. 13, pp. 8291–8299, Jul. 2020, doi: 10.1021/acs.est.0c02444.

[29] S. E. Fenton *et al.*, "Per- and Polyfluoroalkyl Substance Toxicity and Human Health Review: Current State of Knowledge and Strategies for Informing Future Research," *Environ. Toxicol. Chem.*, vol. 00, no. 00, pp. 1–25, 2020, doi: 10.1002/etc.4890.

[30] K. Abraham *et al.*, "Internal exposure to perfluoroalkyl substances (PFASs) and biological markers in 101 healthy 1-year-old children: associations between levels of perfluorooctanoic acid (PFOA) and vaccine response," *Arch. Toxicol.*, vol. 1, p. 3, 2020, doi: 10.1007/s00204-020-02715-4.

[31] C. Y. Lin, H. L. Lee, Y. T. Hwang, and T. C. Su, "The association between total serum isomers of per- and polyfluoroalkyl substances, lipid profiles, and the DNA oxidative/nitrative stress biomarkers in middle-aged Taiwanese adults," *Environ. Res.*, vol. 182, p. 109064, Mar. 2020, doi: 10.1016/j.envres.2019.109064.

[32] V. Barry, A. Winquist, and K. Steenland, "Perfluorooctanoic Acid (PFOA) Exposures and Incident Cancers among Adults Living Near a Chemical Plant," *Environ. Health Perspect.*, vol. 121, no. 11–12, pp. 1313–1318, Nov. 2013, doi: 10.1289/ehp.1306615.

[33] C. T. Vu and T. Wu, "Recent progress in adsorptive removal of per- and poly-fluoroalkyl substances (PFAS) from water/wastewater," *Crit. Rev. Environ. Sci. Technol.*, pp. 1–40, Sep. 2020, doi: 10.1080/10643389.2020.1816125.

[34] I. H. Suffet, "Evaluation of Activated Carbon for Drinking Water Treatment: a National Academy of Science Report.," *J. / Am. Water Work. Assoc.*, vol. 72, no. 1, pp. 41–50, 1980, doi: 10.1002/j.1551-8833.1980.tb04461.x.

[35] H.-J. Butt, K. Graf, and M. Kappl, *Physics and Chemistry of Interfaces*. Berlin: Wiley-VCH, 2003.

[36] C. Eschauzier, E. Beerendonk, P. Scholte-Veenendaal, and P. De Voogt, "Impact of treatment processes on the removal of perfluoroalkyl acids from the drinking water production chain," *Environ. Sci. Technol.*, vol. 46, no. 3, pp. 1708–1715, 2012, doi: 10.1021/es201662b.

[37] S. Takagi *et al.*, "Fate of Perfluorooctanesulfonate and perfluorooctanoate in drinking water treatment processes," *Water Res.*, vol. 45, no. 13, pp. 3925–3932, Jul. 2011, doi: 10.1016/j.watres.2011.04.052.

[38] J. Hölzer *et al.*, "One-year follow-up of perfluorinated compounds in plasma of German residents from Arnsberg formerly exposed to PFOA-contaminated drinking water," *Int. J. Hyg. Environ. Health*, vol. 212, no. 5, pp. 499–504, Sep. 2009, doi: 10.1016/j.ijheh.2009.04.003.

[39] H. Son, T. Kim, H. S. Yoom, D. Zhao, and B. An, "The adsorption selectivity of short

and long per-and polyfluoroalkyl substances (Pfass) from surface water using powder-activated carbon," *Water (Switzerland)*, vol. 12, no. 11, 2020, doi: 10.3390/w12113287.

[40]   S. Deng, Q. Yu, J. Huang, and G. Yu, "Removal of perfluorooctane sulfonate from wastewater by anion exchange resins: Effects of resin properties and solution chemistry," *Water Res.*, vol. 44, no. 18, pp. 5188–5195, Oct. 2010, doi: 10.1016/j.watres.2010.06.038.

[41]   A. Zaggia, L. Conte, L. Falletti, M. Fant, and A. Chiorboli, "Use of strong anion exchange resins for the removal of perfluoroalkylated substances from contaminated drinking water in batch and continuous pilot plants," *Water Res.*, vol. 91, pp. 137–146, Mar. 2016, doi: 10.1016/j.watres.2015.12.039.

[42]   Z. Yang, Y. Zhou, Z. Feng, X. Rui, T. Zhang, and Z. Zhang, "A review on reverse osmosis and nanofiltration membranes for water purification," *Polymers (Basel).*, vol. 11, no. 8, 2019, doi: 10.3390/polym11081252.

[43]   T. D. Appleman *et al.*, "Treatment of poly- and perfluoroalkyl substances in U.S. full-scale water treatment systems," *Water Res.*, vol. 51, pp. 246–255, Mar. 2014, doi: 10.1016/j.watres.2013.10.067.

[44]   J. Thompson *et al.*, "Removal of PFOS, PFOA and other perfluoroalkyl acids at water reclamation plants in South East Queensland Australia," *Chemosphere*, vol. 82, no. 1, pp. 9–17, Jan. 2011, doi: 10.1016/j.chemosphere.2010.10.040.

[45]   C. Y. Tang, Q. S. Fu, A. P. Robertson, C. S. Criddle, and J. O. Leckie, "Use of reverse osmosis membranes to remove perfluorooctane sulfonate (PFOS) from semiconductor wastewater," *Environ. Sci. Technol.*, vol. 40, no. 23, pp. 7343–7349, Dec. 2006, doi: 10.1021/es060831q.

[46]   T. D. Appleman, E. R. V Dickenson, C. Bellona, and C. P. Higgins, "Nanofiltration and granular activated carbon treatment of perfluoroalkyl acids," *J. Hazard. Mater.*, vol. 260, pp. 740–746, Sep. 2013, doi: 10.1016/j.jhazmat.2013.06.033.

[47]   V. Franke, P. McCleaf, K. Lindegren, and L. Ahrens, "Efficient removal of per- And polyfluoroalkyl substances (PFASs) in drinking water treatment: Nanofiltration combined with active carbon or anion exchange," *Environ. Sci. Water Res. Technol.*, vol. 5, no. 11, pp. 1836–1843, Nov. 2019, doi: 10.1039/c9ew00286c.

[48]   C. Boo, Y. Wang, I. Zucker, Y. Choo, C. O. Osuji, and M. Elimelech, "High Performance Nanofiltration Membrane for Effective Removal of Perfluoroalkyl Substances at High Water Recovery," *Environ. Sci. Technol.*, vol. 52, no. 13, pp. 7279–7288, 2018, doi: 10.1021/acs.est.8b01040.

[49]   Y. Wang, I. Zucker, C. Boo, and M. Elimelech, "Removal of Emerging Wastewater Organic Contaminants by Polyelectrolyte Multilayer Nanofiltration Membranes with Tailored Selectivity," *ACS ES&T Eng.*, vol. 1, pp. 404–414, 2020, doi: 10.1021/acsestengg.0c00160.

[50]   N. Belkouteb, V. Franke, P. McCleaf, S. Köhler, and L. Ahrens, "Removal of per- and polyfluoroalkyl substances (PFASs) in a full-scale drinking water treatment plant: Long-term performance of granular activated carbon (GAC) and influence of flow-rate," *Water Res.*, vol. 182, p. 115913, Sep. 2020, doi: 10.1016/j.watres.2020.115913.

[51]   Z. Du *et al.*, "Removal of perfluorinated carboxylates from washing wastewater of

perfluorooctanesulfonyl fluoride using activated carbons and resins," *J. Hazard. Mater.*, vol. 286, pp. 136–143, 2015, doi: 10.1016/j.jhazmat.2014.12.037.

[52] I. M. Militao, F. A. Roddick, R. N. Bergamasco, and L. Fan, "Removing PFAS from aquatic systems using natural and renewable material-based adsorbents: A review," *J. Environ. Chem. Eng.*, p. 105271, Feb. 2021, doi: 10.1016/j.jece.2021.105271.

[53] D. Zhang, Q. He, M. Wang, W. Zhang, and Y. Liang, "Sorption of perfluoroalkylated substances (PFASs) onto granular activated carbon and biochar," *Environ. Technol. (United Kingdom)*, vol. 42, no. 12, pp. 1798–1809, 2021, doi: 10.1080/09593330.2019.1680744.

[54] B. Niu *et al.*, "Regenerable magnetic carbonized Calotropis gigantea fiber for hydrophobic-driven fast removal of perfluoroalkyl pollutants," *Cellulose*, vol. 27, no. 10, pp. 5893–5905, Jul. 2020, doi: 10.1007/s10570-020-03192-9.

[55] S. Islam, M. A. R. Bhuiyan, and M. N. Islam, "Chitin and Chitosan: Structure, Properties and Applications in Biomedical Engineering," *Journal of Polymers and the Environment*, vol. 25, no. 3. Springer New York LLC, pp. 854–866, Sep. 01, 2017, doi: 10.1007/s10924-016-0865-5.

[56] Q. Li, E. T. Dunn, E. W. Grandmaison, and M. F. A. Goosen, "Applications and Properties of Chitosan," 1992. doi: 10.1177/088391159200700406.

[57] Q. Yu, S. Deng, and G. Yu, "Selective removal of perfluorooctane sulfonate from aqueous solution using chitosan-based molecularly imprinted polymer adsorbents," *Water Res.*, vol. 42, no. 12, pp. 3089–3097, Jun. 2008, doi: 10.1016/j.watres.2008.02.024.

[58] Q. Zhang, S. Deng, G. Yu, and J. Huang, "Removal of perfluorooctane sulfonate from aqueous solution by crosslinked chitosan beads: Sorption kinetics and uptake mechanism," *Bioresour. Technol.*, vol. 102, no. 3, pp. 2265–2271, Feb. 2011, doi: 10.1016/j.biortech.2010.10.040.

[59] L. Long, X. Hu, J. Yan, Y. Zeng, J. Zhang, and Y. Xue, "Novel chitosan–ethylene glycol hydrogel for the removal of aqueous perfluorooctanoic acid," *J. Environ. Sci. (China)*, vol. 84, pp. 21–28, Oct. 2019, doi: 10.1016/j.jes.2019.04.007.

[60] H. Nawaz, R. Waheed, M. Nawaz, and D. Shahwar, "Physical and Chemical Modifications in Starch Structure and Reactivity," in *Chemical Properties of Starch*, IntechOpen, 2020.

[61] Y. Gong, L. Wang, J. Liu, J. Tang, and D. Zhao, "Removal of aqueous perfluorooctanoic acid (PFOA) using starch-stabilized magnetite nanoparticles," *Sci. Total Environ.*, vol. 562, pp. 191–200, Aug. 2016, doi: 10.1016/j.scitotenv.2016.03.100.

[62] O. J. Rojas, Ed., *Cellulose Chemistry and Properties: Fibers, Nanocelluloses and Advanced Materials*, vol. 271. Springer, 2016.

[63] S. Deng, Y. Q. Zheng, F. J. Xu, B. Wang, J. Huang, and G. Yu, "Highly efficient sorption of perfluorooctane sulfonate and perfluorooctanoate on a quaternized cotton prepared by atom transfer radical polymerization," *Chemical Engineering Journal*, 2012. https://reader.elsevier.com/reader/sd/pii/S1385894712004524?token=EC755D8427FF 566F6354B2EEF8C94453CB6A7F3D1C1CDE5403BE68D19981CF968FEFD5050D

8598273B0A1943594B5E0E (accessed Feb. 28, 2021).

[64] M. Bevilacqua, F. E. Ciarapica, G. Mazzuto, and C. Paciarotti, "Environmental analysis of a cotton yarn supply Chain," *J. Clean. Prod.*, vol. 82, pp. 154–165, Nov. 2014, doi: 10.1016/j.jclepro.2014.06.082.

[65] B. Niu *et al.*, "A Comparative Study for Removal of Perfluorooctanoic Acid Using Three Kinds of N-polymer Functionalized Calotropis Gigantea Fiber," *J. Nat. Fibers*, 2020, doi: 10.1080/15440478.2020.1798848.

[66] M. Ateia *et al.*, "Rapid Removal of Poly- and Perfluorinated Alkyl Substances by Poly(ethylenimine)-Functionalized Cellulose Microcrystals at Environmentally Relevant Conditions," *Environ. Sci. Technol. Lett.*, vol. 5, no. 12, pp. 764–769, 2018, doi: 10.1021/acs.estlett.8b00556.

[67] T. F. Cova, D. Murtinho, A. A. C. C. Pais, and A. J. M. Valente, "Combining cellulose and cyclodextrins: Fascinating designs for materials and pharmaceutics," *Front. Chem.*, vol. 6, no. JUL, p. 271, Jul. 2018, doi: 10.3389/fchem.2018.00271.

[68] A. Z. M. Badruddoza, B. Bhattarai, and R. P. S. Suri, "Environmentally Friendly β-Cyclodextrin-Ionic Liquid Polyurethane-Modified Magnetic Sorbent for the Removal of PFOA, PFOS, and Cr(VI) from Water," *ACS Sustain. Chem. Eng.*, vol. 5, no. 10, pp. 9223–9232, 2017, doi: 10.1021/acssuschemeng.7b02186.

[69] L. Xiao, Y. Ling, A. Alsbaiee, C. Li, D. E. Helbling, and W. R. Dichtel, "β-Cyclodextrin Polymer Network Sequesters Perfluorooctanoic Acid at Environmentally Relevant Concentrations," *J. Am. Chem. Soc.*, vol. 139, no. 23, pp. 7689–7692, 2017, doi: 10.1021/jacs.7b02381.

[70] L. Xiao *et al.*, "Cross-linker Chemistry Determines the Uptake Potential of Perfluorinated Alkyl Substances by β-Cyclodextrin Polymers," *Macromolecules*, vol. 52, pp. 3747–3752, 2019, doi: 10.1021/acs.macromol.9b00417.

[71] N. Mohammed, N. Grishkewich, R. M. Berry, and K. C. Tam, "Cellulose nanocrystal–alginate hydrogel beads as novel adsorbents for organic dyes in aqueous solutions," *Cellulose*, vol. 22, no. 6, pp. 3725–3738, 2015, doi: 10.1007/s10570-015-0747-3.

[72] N. Mohammed, N. Grishkewich, H. A. Waeijen, R. M. Berry, and K. C. Tam, "Continuous flow adsorption of methylene blue by cellulose nanocrystal-alginate hydrogel beads in fixed bed columns," *Carbohydr. Polym.*, vol. 136, pp. 1194–1202, 2016, doi: 10.1016/j.carbpol.2015.09.099.

[73] F. Zhang, M. S. Islam, R. M. Berry, and K. C. Tam, "β-Cyclodextrin-Functionalized Cellulose Nanocrystals and Their Interactions with Surfactants," *ACS Omega*, vol. 4, no. 1, pp. 2102–2110, 2019, doi: 10.1021/acsomega.8b02534.

[74] M. C. Hansen, M. H. Børresen, M. Schlabach, and G. Cornelissen, "Sorption of perfluorinated compounds from contaminated water to activated carbon," *J. Soils Sediments*, vol. 10, no. 2, pp. 179–185, 2010, doi: 10.1007/s11368-009-0172-z.

[75] N. Mohammed, N. Grishkewich, and K. C. Tam, "Cellulose nanomaterials: Promising sustainable nanomaterials for application in water/wastewater treatment processes," *Environmental Science: Nano*, vol. 5, no. 3. Royal Society of Chemistry, pp. 623–658, Mar. 15, 2018, doi: 10.1039/c7en01029j.

[76] R. J. Moon, A. Martini, J. Nairn, J. Simonsen, and J. Youngblood, "Cellulose nanomaterials review: Structure, properties and nanocomposites," *Chem. Soc. Rev.*,

vol. 40, no. 7, pp. 3941–3994, Jun. 2011, doi: 10.1039/c0cs00108b.

[77] R. Batmaz, N. Mohammed, M. Zaman, G. Minhas, R. M. Berry, and K. C. Tam, "Cellulose nanocrystals as promising adsorbents for the removal of cationic dyes," *Cellulose*, vol. 21, no. 3, pp. 1655–1665, Jan. 2014, doi: 10.1007/s10570-014-0168-8.

[78] H. Qiao *et al.*, "Effective removal of cationic dyes using carboxylate-functionalized cellulose nanocrystals," *Chemosphere*, vol. 141, pp. 297–303, 2015, doi: 10.1016/j.chemosphere.2015.07.078.

[79] P. Liu, P. F. Borrell, M. Božič, V. Kokol, K. Oksman, and A. P. Mathew, "Nanocelluloses and their phosphorylated derivatives for selective adsorption of Ag+, Cu2+ and Fe3+ from industrial effluents," *J. Hazard. Mater.*, vol. 294, pp. 177–185, 2015, doi: 10.1016/j.jhazmat.2015.04.001.

[80] M. Zaman, H. Xiao, F. Chibante, and Y. Ni, "Synthesis and characterization of cationically modified nanocrystalline cellulose," *Carbohydr. Polym.*, vol. 89, no. 1, pp. 163–170, Jun. 2012, doi: 10.1016/j.carbpol.2012.02.066.

[81] M. Hasani, E. D. Cranston, G. Westman, and D. G. Gray, "Cationic surface functionalization of cellulose nanocrystals," *Soft Matter*, vol. 4, no. 11, pp. 2238–2244, 2008, doi: 10.1039/b806789a.

[82] N. Lin and A. Dufresne, "Supramolecular hydrogels from in situ host-guest inclusion between chemically modified cellulose nanocrystals and cyclodextrin," *Biomacromolecules*, vol. 14, no. 3, pp. 871–880, 2013, doi: 10.1021/bm301955k.

[83] F. Roselet, J. Burkert, and P. C. Abreu, "Flocculation of Nannochloropsis oculata using a tannin-based polymer: Bench scale optimization and pilot scale reproducibility," *Biomass and Bioenergy*, vol. 87, pp. 55–60, Apr. 2016, doi: 10.1016/j.biombioe.2016.02.015.

[84] D. P. Facchi *et al.*, "Polyelectrolyte complexes based on alginate/tanfloc: Optimization, characterization and medical application," *Int. J. Biol. Macromol.*, vol. 103, pp. 129–138, Oct. 2017, doi: 10.1016/j.ijbiomac.2017.05.033.

[85] B.-B. Lee, P. Ravindra, and E.-S. Chan, "Size and Shape of Calcium Alginate Beads Produced by Extrusion Dripping," *Chem. Eng. Technol.*, vol. 36, no. 10, p. n/a-n/a, Sep. 2013, doi: 10.1002/ceat.201300230.

[86] N. Lin, A. Gè, D. Wouessidjewe, J. Huang, and A. Dufresne, "Biocompatible Double-Membrane Hydrogels from Cationic Cellulose Nanocrystals and Anionic Alginate as Complexing Drugs Codelivery," 2016, doi: 10.1021/acsami.6b00555.

[87] R. L. Birru *et al.*, "A pathway level analysis of PFAS exposure and risk of gestational diabetes mellitus," *Environ. Heal. A Glob. Access Sci. Source*, vol. 20, no. 1, pp. 1–16, Dec. 2021, doi: 10.1186/s12940-021-00740-z.

[88] L. Lind, B. Zethelius, S. Salihovic, B. Van Bavel, and P. M. Lind, "Circulating levels of perfluoroalkyl substances and prevalent diabetes in the elderly," *Diabetologia*, vol. 57, no. 3, pp. 473–479, Mar. 2014, doi: 10.1007/s00125-013-3126-3.

[89] B. N. Conway, A. N. Badders, T. Costacou, J. M. Arthur, and K. E. Innes, "Perfluoroalkyl substances and kidney function in chronic kidney disease, anemia, and diabetes," *Diabetes, Metab. Syndr. Obes. Targets Ther.*, vol. 11, pp. 707–716, 2018, doi: 10.2147/DMSO.S173809.

[90] L. Q. Wang *et al.*, "Perfluoroalkyl substance pollutants activate the innate immune

system through the AIM2 inflammasome," *Nat. Commun.*, vol. 12, no. 1, pp. 1–17, Dec. 2021, doi: 10.1038/s41467-021-23201-0.

[91]   J. J. Hefferren and C. Dietz, "Determination of quaternary ammonium compounds," *J. Pharm. Sci.*, vol. 50, no. 6, pp. 535–536, 1961, doi: 10.1002/jps.2600500620.

[92]   G. S. Dmitriev, L. N. Zanaveskin, and S. N. Khadzhiev, "Effect of sodium chloride on the solubility and hydrolysis of epichlorohydrin in water," *Russ. Chem. Bull.*, vol. 67, no. 9, pp. 1627–1630, 2018, doi: 10.1007/s11172-018-2269-2.

[93]   W. Li, J. Zhou, L. Zhang, H. Corke, and L. Yang, "Factors affecting the determination of β-cyclodextrin by phenolphthalein spectrophotometry," *Anal. Lett.*, vol. 29, no. 7, pp. 1201–1213, 1996, doi: 10.1080/00032719608001469.

[94]   Q. Lin, Y. Wu, X. Jiang, F. Lin, X. Liu, and B. Lu, "Removal of bisphenol A from aqueous solution via host-guest interactions based on beta-cyclodextrin grafted cellulose bead," *Int. J. Biol. Macromol.*, vol. 140, pp. 1–9, Nov. 2019, doi: 10.1016/j.ijbiomac.2019.08.116.

[95]   M. A. Al-Ghouti and R. S. Al-Absi, "Mechanistic understanding of the adsorption and thermodynamic aspects of cationic methylene blue dye onto cellulosic olive stones biomass from wastewater," *Sci. Rep.*, vol. 10, no. 1, pp. 1–18, Sep. 2020, doi: 10.1038/s41598-020-72996-3.

[96]   H. I. Albroomi, M. A. Elsayed, A. Baraka, and M. A. Abdelmaged, "Batch and fixed-bed adsorption of tartrazine azo-dye onto activated carbon prepared from apricot stones," *Appl. Water Sci. 2016 74*, vol. 7, no. 4, pp. 2063–2074, Feb. 2016, doi: 10.1007/S13201-016-0387-2.

[97]   M. Müller, "Sizing, shaping and pharmaceutical applications of polyelectrolyte complex nanoparticles," in *Advances in Polymer Science*, vol. 256, Springer, Berlin, Heidelberg, 2014, pp. 197–260.

[98]   Y. Nishio, J. Sato, and K. Sugimura, "Liquid Crystals of Cellulosics: Fascinating Ordered Structures for the Design of Functional Material Systems," *Adv. Polym. Sci.*, vol. 271, pp. 241–286, 2015, doi: 10.1007/12_2015_308.

[99]   H. Wang and M. Roman, "Formation and properties of chitosan-cellulose nanocrystal polyelectrolyte-macroion complexes for drug delivery applications," *Biomacromolecules*, vol. 12, no. 5, pp. 1585–1593, 2011, doi: 10.1021/bm101584c.

[100] A. Gupta, W. Simmons, G. T. Schueneman, D. Hylton, and E. A. Mintz, "Rheological and thermo-mechanical properties of poly(lactic acid)/lignin-coated cellulose nanocrystal composites," *ACS Sustain. Chem. Eng.*, vol. 5, no. 2, pp. 1711–1720, 2017, doi: 10.1021/acssuschemeng.6b02458.

[101] O. Hadizat Ajao, "Physicochemical Treatment of Combined Sewer Oveflow using Physicochemical Treatment of Combined Sewer Oveflow using Natural Polymers," University of Windsor, 2016.

[102] W. H. Xie, W. Y. Shiu, and D. Mackay, "A review of the effect of salts on the solubility of organic compounds in seawater," *Mar. Environ. Res.*, vol. 44, no. 4, pp. 429–444, Dec. 1997, doi: 10.1016/S0141-1136(97)00017-2.

[103] R. Nandini and B. Vishalakshi, "A study of interaction of methyl orange with some polycations," *E-Journal Chem.*, vol. 9, no. 1, pp. 1–14, 2012, doi: 10.1155/2012/343928.

[104] J. D. Giraldo, V. H. Campos-Requena, and B. L. Rivas, "Chitosan–tripolyphosphate bead: the interactions that govern its formation," *Polym. Bull. 2018 768*, vol. 76, no. 8, pp. 3879–3903, Oct. 2018, doi: 10.1007/S00289-018-2574-9.